LETTERS
https://doi.org/10.1038/s41564-019-0569-4
nature microbiology

Cooking shapes the structure and function of the gut microbiome

Rachel N. Carmody[1,2,3*], Jordan E. Bisanz[1], Benjamin P. Bowen[4,5], Corinne F. Maurice[2,6], Svetlana Lyalina[7], Katherine B. Louie[4,5], Daniel Treen[4,5], Katia S. Chadaideh[3], Vayu Maini Rekdal[8], Elizabeth N. Bess[1], Peter Spanogiannopoulos[1], Qi Yan Ang[1], Kylynda C. Bauer[2], Thomas W. Balon[9], Katherine S. Pollard[7], Trent R. Northen[4,5] and Peter J. Turnbaugh[1,2,10*]

Diet is a critical determinant of variation in gut microbial structure and function, outweighing even host genetics[1–3]. Numerous microbiome studies have compared diets with divergent ingredients[1–5], but the everyday practice of cooking remains understudied. Here, we show that a plant diet served raw versus cooked reshapes the murine gut microbiome, with effects attributable to improvements in starch digestibility and degradation of plant-derived compounds. Shifts in the gut microbiota modulated host energy status, applied across multiple starch-rich plants, and were detectable in humans. Thus, diet-driven host–microbial interactions depend on the food as well as its form. Because cooking is human-specific, ubiquitous and ancient[6,7], our results prompt the hypothesis that humans and our microbiomes co-evolved under unique cooking-related pressures.

Heat alters the physicochemical properties of foods in ways that could impact the gut microbiome. Cooking increases the ileal digestibility of carbohydrates by gelatinizing starch[6,8], reducing the quantity reaching the colon, where the most numerous microbial community resides, and potentially affecting the fermentation capability of amylolytic gut bacteria[9]. Cooking can also denature antimicrobial compounds present naturally in food or introduced through agriculture[10,11], thus limiting their bioactivity. Here, we interrogate the impact of cooking on the gut microbiome, as well as downstream impacts on host energy status.

To gauge the overall influence of cooking, we conducted 16S rDNA sequencing and shotgun sequencing of microbial RNA in distal gut samples collected from conventional mice reared for 5 days on organic lean beef or organic sweet potato served raw or cooked (Supplementary Fig. 1a and Supplementary Table 1a). These foods were chosen for their importance in past and present human diets[12], their diverse macronutrient profiles, and prior evidence of cooking influencing nutrient bioavailability[6], antimicrobial properties[13] and host energy balance[12]. Among mice fed cooked meals, half were free-fed and half received a restricted ration calibrated to produce ~1 g weight loss, allowing us to investigate the effects of cooking separately from those of changes in host energy gain associated with cooking. Ration restriction led to predictable reductions in caloric intake and body mass (Supplementary Fig. 1b,c). Among free-fed tuber diets, cooked diets were associated with lower caloric intakes but higher body mass outcomes, confirming that cooking increases net energy gain from this substrate[12]. We observed rapid and reproducible changes in gut microbial structure and function among mice fed meat versus tuber (Fig. 1a,b, Supplementary Fig. 1d–h, Supplementary Table 2a–c and Supplementary Notes), with effects paralleling those observed in an earlier study of humans consuming animal-based versus plant-based diets[5].

Cooking impacted the gut microbiome differently on meat versus tuber diets. The gut microbiomes of mice fed raw and cooked meat were similar in composition and transcriptional profile (Fig. 1b–d and Supplementary Fig. 1d,e), although we were still able to detect 12 modules and 68 orthologous groups with significant differences in expression (Supplementary Table 3a,b). By contrast, the gut microbiomes of mice fed raw and cooked tuber were fundamentally distinct. Microbial community structure in tuber-fed mice was explained primarily by processing, a pattern evident within 24 h of diet initiation ($R = 0.624$, $P < 0.05$, analysis of similarities $(\text{ANOSIM})_{\text{day1samples}}$; Fig. 1e). Consuming raw versus cooked tuber led to lower α-diversity, marginally lower bacterial abundance and a rise in the relative proportion of Bacteroidetes, a phylum with broad capabilities for glycan degradation[14,15] (Fig. 1d,f–h and Supplementary Table 4a). By contrast, gut microbial community structure on the cooked tuber diet resembled that at baseline, when mice were consuming a chow composed primarily of cooked plants. Because raw-fed mice lost more weight than cooked-fed mice (Supplementary Fig. 1c), we tested and confirmed that the effects of processing dominated those of experimental factors related to energy status, such as ration restriction and changes in body mass over various timescales (Supplementary Table 4b), a pattern also apparent in RNAseq-based analysis of host tissues[7]. Community-wide gene expression profiles clustered by processing for tuber diets (Fig. 1b and Supplementary Fig. 1d), representing significant differences in 174 modules and 1,419 orthologous groups (Supplementary Table 4c,d). The microbial communities of raw-fed hosts showed higher expression of genes for the metabolism of starch and sugar (ko00051, ko00500) and xenobiotic compounds

[1]Department of Microbiology & Immunology, University of California San Francisco, San Francisco, CA, USA. [2]Center for Systems Biology, Harvard University, Cambridge, MA, USA. [3]Department of Human Evolutionary Biology, Harvard University, Cambridge, MA, USA. [4]Environmental Genomics and Systems Biology Division, Lawrence Berkeley National Laboratory, Berkeley, CA, USA. [5]DOE Joint Genome Institute, Walnut Creek, CA, USA. [6]Department of Microbiology & Immunology, Microbiome and Disease Tolerance Centre, McGill University, Montreal, Quebec, Canada. [7]Gladstone Institutes, University of California San Francisco, San Francisco, CA, USA. [8]Department of Chemistry and Chemical Biology, Harvard University, Cambridge, MA, USA. [9]Department of Medicine, Metabolic Phenotyping Core and In Vivo Imaging System Core, Boston University, Boston, MA, USA. [10]Chan Zuckerberg Biohub, San Francisco, CA, USA. *e-mail: carmody@fas.harvard.edu; peter.turnbaugh@ucsf.edu

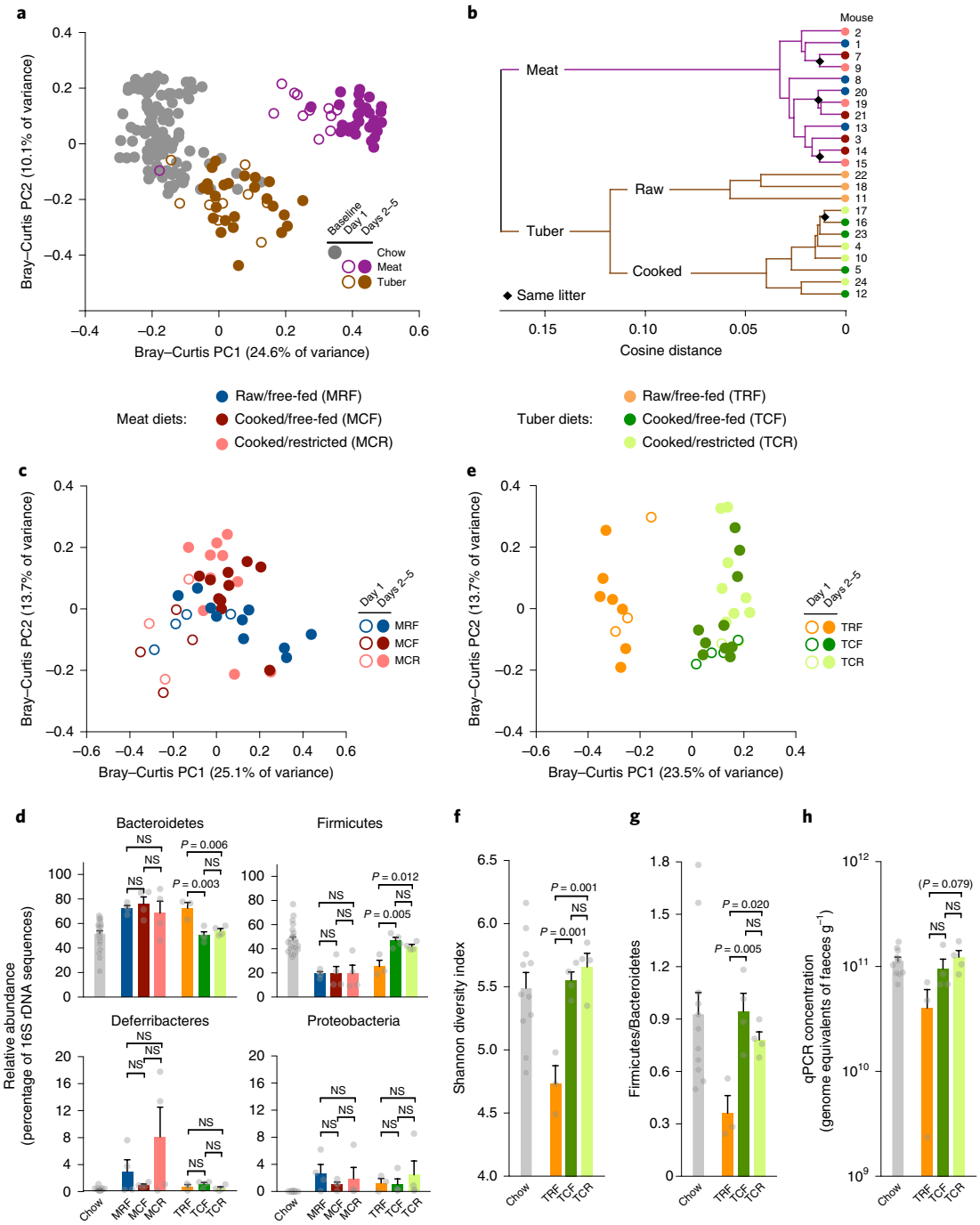

Fig. 1 | Cooking impacts gut microbiota structure and function in tuber-fed mice. a, Bray–Curtis principal coordinate plot showing that diets of meat or tuber rapidly and reproducibly reshaped the murine gut microbiota (meat, $n=12$; tuber, $n=11$). Clusters indicate that diet substrate was a strong predictor of community structure, with communities consistently responding within 24 h after the switch from chow to whole-food diets. Note that the day 1 meat sample clustering with chow reflects a mouse that did not consume any meat within the first 24 h. **b**, Hierarchical clustering of RNAseq-based gut microbial gene expression (Ward.D2 algorithm). Clusters indicate that expression profiles were strongly differentiated by diet substrate and, within tuber diets, by cooking. **c**, Bray–Curtis principal coordinate plot showing that gut microbial communities were similar among mice fed meat served raw/free-fed (MRF), cooked/free-fed (MCF) or cooked/restricted (MCR) ($n=4$ animals per treatment; Supplementary Fig. 1a). **d**, Relative abundance of the four most abundant bacterial phyla in the distal guts of mice fed meat or tuber served raw or cooked versus a baseline diet of chow, incorporating a single endpoint sample per mouse ($n=3$–4 animals per treatment). **e**, Bray–Curtis principal coordinate plot showing that gut microbial communities were clearly distinct among mice fed tuber served raw/free-fed (TRF) versus cooked/free-fed (TCF) or cooked/restricted (TCR) ($n=4$ animals per treatment), a pattern established within 24 h of diet administration. TCF and TCR samples clustered together, confirming that effects were attributable to cooking rather than cooking-associated differences in host energy balance. **f–h**, Compared with cooked tuber, the raw tuber diet produced a unique profile that included lower α-diversity, as judged by the Shannon diversity index (**f**), a lower proportion of bacteria from the Firmicutes versus Bacteroidetes phyla (**g**) and qualitatively lower bacterial abundance as assessed by quantitative PCR (qPCR) (**h**). In **f–h**, comparisons across tuber treatment groups reflect a single endpoint sample per individual ($n=3$–4 animals per treatment). In **d** and **f–h**, data are presented as mean ± s.e.m.; statistics reflect one-way analysis of variance (ANOVA) with Holm–Sidak correction for multiple comparisons. NS, not significant.

(ko00980, ko00982) (Supplementary Table 4c), consistent with our expectations of lower digestibility and higher xenobiotic load in raw sweet potato. In addition, when compared against the Carbohydrate Active Enzymes (CAZy) database, β-amylase (GH14/EC3.2.1.2) emerged as one of two enzyme families distinguishing raw versus cooked tuber samples (false discovery rate, FDR < 0.05), the other being a broad glycosyltransferase family (GT2).

Apart from water, raw sweet potato tubers are composed principally of starch (44% of dry mass; Supplementary Table 1a). Cooking transforms this starch through gelatinization, whereby native semi-crystalline granules of amylopectin and amylose are degraded into amorphous structures susceptible to amylase digestion, increasing their absorption in the small intestine[6,8,16]. We reasoned that microbial communities could be sensitive to the reduced fraction of cooked starch reaching the colon, and its altered structure[17], and therefore tested whether we could recapitulate the effects of raw versus cooked tuber diets on the gut microbiome by manipulating starch digestibility. We reared conventional mice for 28 days on macronutrient-matched chows differing only in the ileal digestibility of their starch fraction (50% wt/wt) (Supplementary Fig. 2a and Supplementary Table 1b). Despite the lesser chow and starch consumption (Fig. 2a and Supplementary Fig. 2b), mice consuming high-digestibility starch (HDS) had body masses and fat levels similar to those of mice consuming low-digestibility starch (LDS) (Fig. 2b and Supplementary Fig. 2c), a result reflecting the higher energetic returns to the host of starch digested in the small intestine versus the colon[18]. Mirroring patterns observed on the raw tuber diet, LDS- versus HDS-feeding led to microbial community divergence ($R = 0.840$, $P < 0.01$, $\mathrm{ANOSIM}_{\mathrm{day28samples}}$; Fig. 2c), with the LDS diet resulting in lower bacterial abundance, lower proportions of Firmicutes versus Bacteroidetes, and a trend towards lower α-diversity (Fig. 2d,e, Supplementary Fig. 2d and Supplementary Table 5). We replicated this experiment in germ-free mice colonized with a common inoculum, confirming higher faecal energy loss in LDS-fed versus HDS-fed animals, and observing changes in community structure, α-diversity and Firmicutes/Bacteroidetes relative abundance that paralleled those observed in conventional animals (Fig. 2f–j, Supplementary Fig. 2e–h and Supplementary Table 5). Thus, gut microbial responses to altered starch digestibility recapitulated key patterns observed in mice fed raw versus cooked tuber.

If starch digestibility is a key factor shaping the gut microbiota, we should expect to see stronger effects of cooking in starch-rich foods versus low-starch foods, and, among starch-rich foods, greater effects of cooking where the ileal digestibility of the raw starch is lower. To test these ideas, we conducted an expanded set of experiments in sweet potato and five other common plant foods: white potato, corn, pea, carrot and beet. These foods were chosen to include a mix of starch-rich (sweet potato, white potato, corn and pea) and low-starch (carrot and beet) items, and starches with lower (sweet potato and white potato) and higher (corn and pea) digestibility when raw (Supplementary Fig. 3a–d and Supplementary Tables 1c and 6). These experiments support the importance of starch digestibility as a driver of microbial changes with cooking; however, we cannot exclude some contribution of diet-induced changes to host physiology. For both α-diversity and β-diversity, we found evidence of divergent microbial signatures for sweet potato and white potato, the foods with a high quantity of low-digestibility starch (Fig. 2k,l). In contrast, there were no consistent microbial effects of cooking for low-starch foods (carrot and beet) or foods with a high quantity of high-digestibility starch (corn and pea), despite all foods showing detectable intervention effects (Fig. 2k,l and Supplementary Fig. 3e–g).

Heat can also affect non-starch plant components, including defence compounds[10]. To gauge the potential impact of heat-sensitive plant-derived antimicrobial compounds on the gut microbiome, we used fluorescent cell staining[19,20] to examine gut microbial physiology in mice consuming diets of raw or cooked tuber, chow, or chow plus the broad-spectrum antibiotic ampicillin as a positive control (Fig. 3a). Using flow cytometry, we quantified microbial cells in fresh faecal pellets that exhibited membrane damage (propidium iodide (PI) stain) and/or high nucleic acid content (HNA), indicating cellular activity[19] (SYBR Green I stain). Before diet treatment, all mice displayed low levels of microbial cell damage (proportion of PI+ cells, 6.6 ± 1.6%), high levels of activity (proportion of HNA cells, 50.3 ± 8.4%) and dense bacterial abundances ($4.8 \times 10^9 \pm 1.4 \times 10^9$ cells per ml suspension). Relative to baseline values, the raw tuber and ampicillin-treated groups exhibited increases in gut microbial cell damage and decreases in cell activity and bacterial load that were not observed in the cooked tuber or standard chow groups (Fig. 3b–d).

Metabolomics was used to identify putative antimicrobial factors. Although each of the six plant foods studied had a distinct composition, we found a consistent signature of cooking in each substrate (Fig. 3e and Supplementary Fig. 4a). Global analysis of metabolite features revealed that cooking caused compositional changes in all plant foods, with sweet potato and white potato exhibiting the greatest shifts and skew towards reduced metabolite complexity (Fig. 3f and Supplementary Fig. 4b). Using targeted analysis, a total of 246 total compounds were identified, 185 of which were high-confidence unambiguous assignments and 51 of which were significantly different (FDR < 0.1 and $|\log_2 \mathrm{FC}| > 1$) in raw versus cooked sweet potato and/or white potato (Fig. 3g, Supplementary Fig. 4c and Supplementary Table 7). We prioritized candidates with prior evidence of antimicrobial activity and sensitivity to heat-induced degradation (Supplementary Table 8). Chlorogenic acid and its downstream metabolite caffeic acid emerged as promising candidates; however, in vitro, ex vivo and in vivo assays failed to confirm antimicrobial effects in these isolated compounds (Supplementary Fig. 5a–i and Supplementary Table 9). Multiple additional compounds with known antibacterial effects were significantly decreased in cooked tubers, including 4-hydroxycinnamic acid, ferulate and vanillic acid[21–23]; these and others may act in concert to impact gut bacterial physiology. Together, these results are consistent with our observation that raw tubers upregulate microbial pathways for xenobiotic metabolism (Supplementary Table 4c) and the broader hypothesis that plant-derived compounds with heat-sensitive antimicrobial properties impair gut microbial physiology. However, it remains possible that gut microbial physiology is sensitive to additional cooking-related factors acting in concert, such as altered physical access to nutrients, changes in microbe–microbe interactions and host-driven changes in the luminal environment.

Next, we sought to determine the consequences of cooking-induced shifts in the gut microbiota for host energy balance. Reduced starch digestibility in the small intestine might select for colonic bacteria capable of fermenting starch or shape other host–microbial interactions affecting energy balance. Increased antimicrobial activity arising from higher xenobiotic load may also confer anabolic effects akin to those observed with low-dose antibiotic administration[24,25]. To assess the effects on host energy balance, we transplanted gut microbiotas conditioned on raw versus cooked tuber diets into germ-free mice fed chow (Fig. 4a). The gut microbial communities of donors and recipients clustered together (Supplementary Fig. 6a), with donor diet explaining the majority of variation observed in recipient communities at all timepoints following the first transitional 24 h post-gavage. As expected, controlling for routine colonization-associated decreases in caecal effluent, inoculation had positive effects on body mass and adiposity (Fig. 4b–d). Notably, the recipients of the raw-fed gut microbiota exhibited increased body mass and adiposity relative to cooked-fed recipients (Fig. 4c,d), despite producing faeces with higher energy content (Supplementary Fig. 6b). This seeming contradiction could be explained by increased caloric intake in the raw-fed microbiota

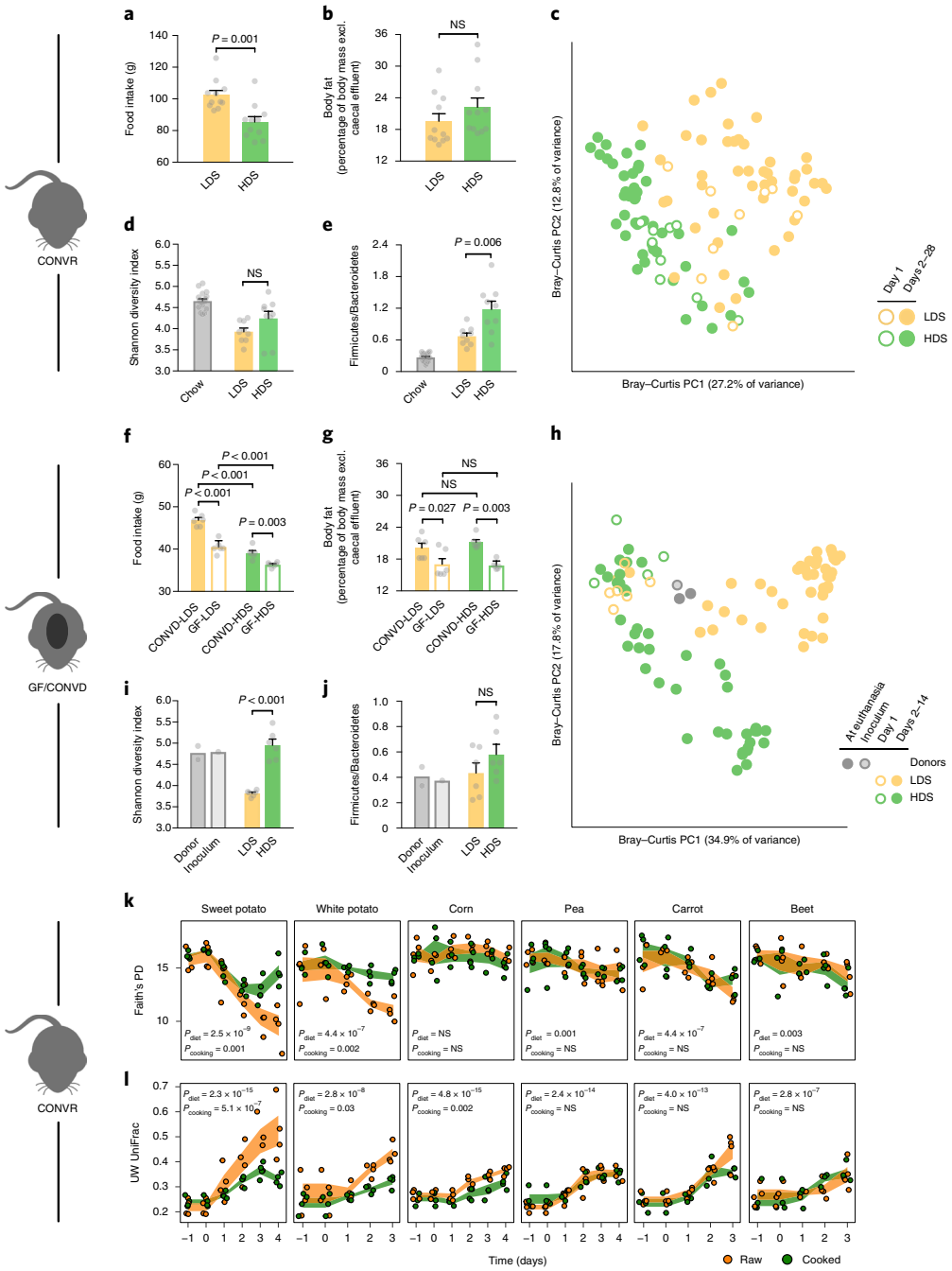

Fig. 2 | Starch digestibility drives cooking-related changes in gut microbial community structure. a–j, Host phenotype and microbial community changes in conventionally raised mice (CONVR) fed semi-purified diets with LDS or HDS for 28 days ($n = 11$ animals per treatment; Supplementary Fig. 2a) (**a**–**e**) or germ-free (GF) or conventionalized (CONVD) mice fed LDS or HDS diets for 14 days (GF $n = 6$ and CONVD $n = 6$ animals per treatment; Supplementary Fig. 2e) (**f**–**j**). Cumulative food intake (**a**,**f**) over the feeding trial. Body fat as a percentage of body mass (**b**,**g**), measured by EchoMRI. Bray–Curtis principal coordinate plots (**c**,**h**) showing that LDS and HDS diets induced distinct gut microbial communities. In **h**, we include data from donor faeces and the pooled inoculum. Recipient microbial communities cluster with donor samples for 24 h post-inoculation, then diverge by diet. Mirroring the patterns observed in mice fed raw tuber (Fig. 1f,g), the LDS diet was associated with a consistent trend towards lower α-diversity (**d**,**i**) and lower proportions of Firmicutes versus Bacteroidetes (**e**,**j**) compared with the HDS diet. Bar charts show mean ± s.e.m. and reflect a single endpoint sample per individual; statistics in **a**,**b**,**d**,**e**,**i**,**j** reflect two-tailed unpaired *t*-tests, and statistics in **f**,**g** reflect two-way ANOVA with Holm–Sidak correction for multiple comparisons. **k**,**l**, Gut microbial profiles in mice fed common plant foods served raw (orange) or cooked (green), including starchy (sweet potato, white potato, corn and pea) and non-starchy (carrot and beet) foods, and foods with relatively low-digestibility (sweet potato and white potato) and high-digestibility (corn and pea) starch ($n = 4$ animals per treatment; total $n = 48$): Faith's phylogenetic diversity (PD; **k**) and unweighted (UW) UniFrac distances (**l**). Points reflect individual distances from baseline, with the band reflecting mean ± s.e.m. In **k**, all plant foods except corn altered Faith's phylogenetic diversity compared to the chow baseline. However, only sweet potato and white potato differed in α-diversity when served raw versus cooked. In **l**, similarly, all plant foods altered gut microbial community structure, as measured by unweighted UniFrac distances from baseline. However, the effects of cooking on β-diversity were only significant in sweet potato, white potato and corn. Statistics in **k** and **l** reflect linear mixed effect models analysing the effect of time on diet (P_{diet}) and its interaction with food preparation ($P_{cooking}$). NS, not significant.

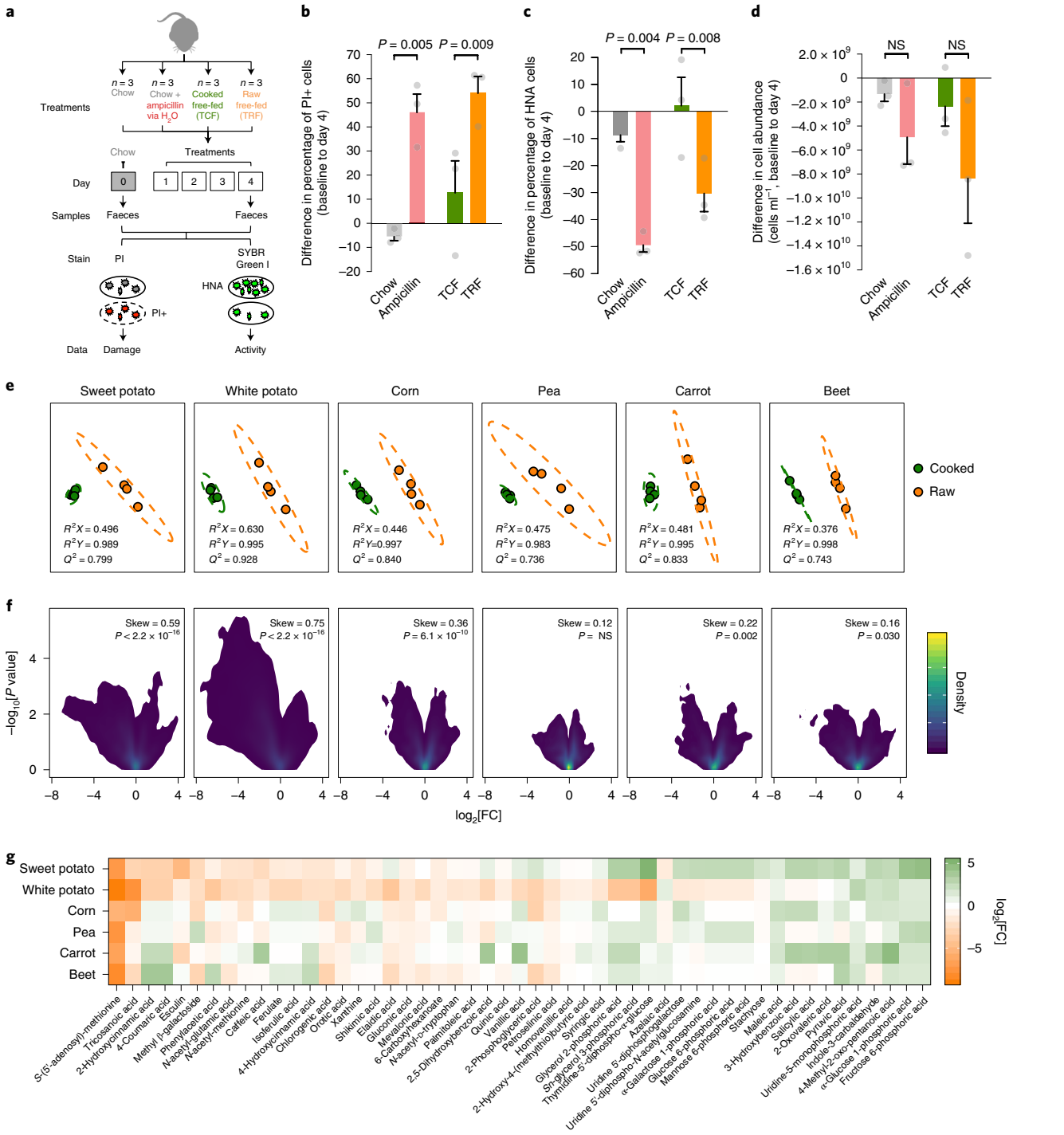

Fig. 3 | The raw tuber diet impairs gut microbial physiology. a, We assessed treatment-induced differences in gut microbial physiology and bacterial load among mice reared for 4 days on chow, chow plus 0.1% wt/wt ampicillin via water supply (positive control) or ad libitum diets of tuber served cooked (TCF) or raw (TRF) ($n = 3$ animals per treatment). **b**, Percentage of cells in the faecal gut microbial community with membrane damage as indexed by PI staining (PI+). **c**, Percentage of cells in the faecal gut microbial community with relatively high activity levels, based on HNA content. **d**, Number of bacterial cells per ml of faecal suspension. The gut microbial communities of mice fed chow and cooked tuber remained close to their baseline values across all three indices of microbial community robustness. By contrast, those of mice fed ampicillin or raw tuber exhibited marked impairment, with high rates of membrane damage, low proportions of highly active cells and reduced bacterial load. In **b**–**d**, one data point is reflected per individual. Data are presented as mean ± s.e.m. and statistics reflect one-way ANOVA with Holm–Sidak correction for multiple comparisons. **e**–**g**, Metabolomics analysis of six plant foods in raw and cooked forms ($n = 4$, animals per treatment; total, $n = 48$) highlights candidates for the antimicrobial effects of raw plant food diets: partial least-squares discriminant analysis plots showing that cooking affects compound abundance across all six food types (**e**); density volcano plots demonstrating that cooking overwhelmingly reduces the abundances of metabolites detected by mass spectrometry in sweet potato and white potato (**f**; skewedness (D'Agostino test) is denoted for each plant food); and a heat map of identified metabolites significantly altered by cooking (**g**, FDR < 0.1 and $|\log_2 FC| > 1$ in sweet potato and/or white potato). Individual features and their methods of quantification (hydrophilic interaction liquid chromatography (HILIC) or C18 chromatography) are listed in Supplementary Table 7. NS, not significant; FC, fold change; R^2X, variance explained for x variable; R^2Y, variance explained for y variable; Q^2, predictive performance.

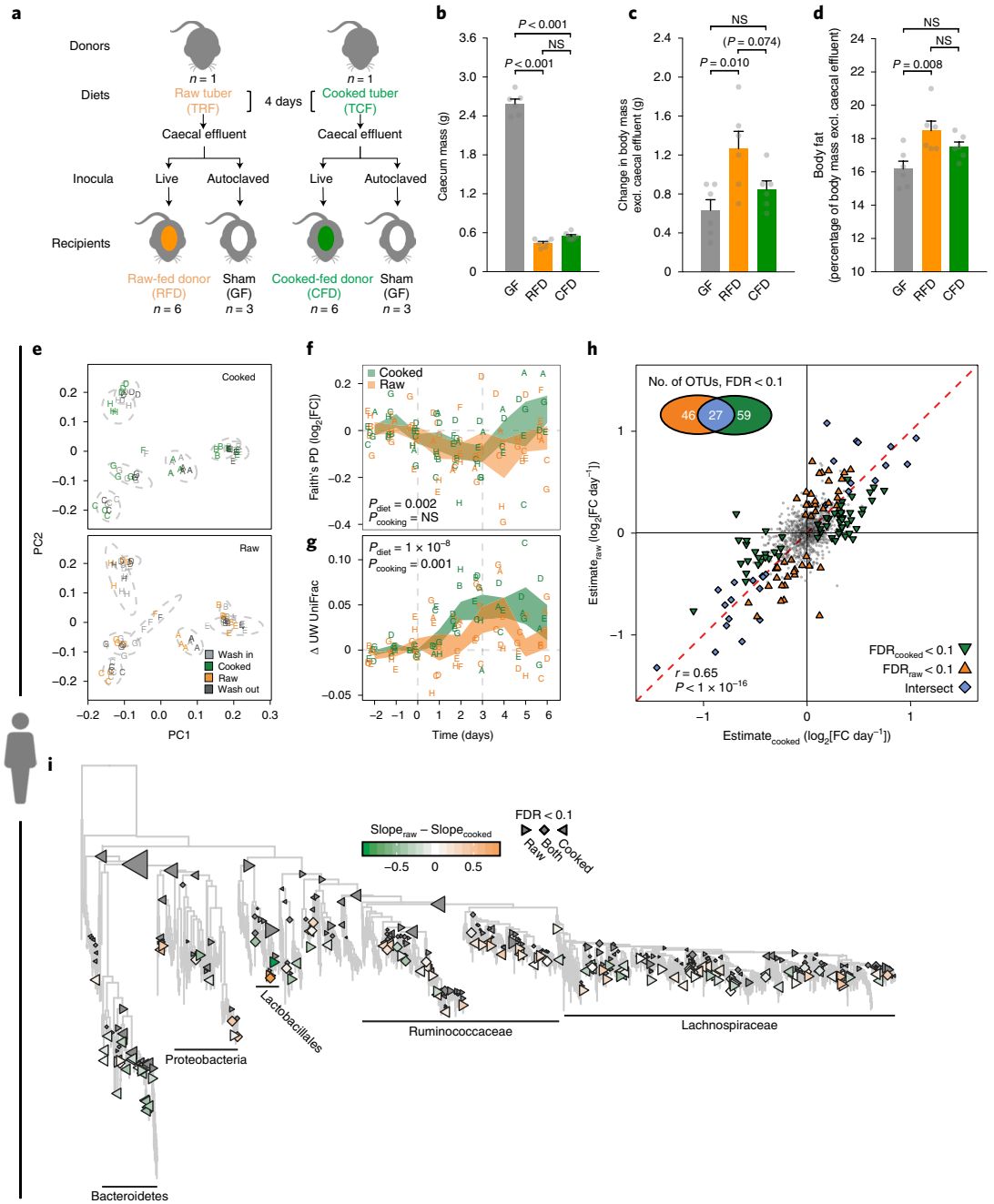

Fig. 4 | Cooking-induced changes in the gut microbiota are ecologically significant. a–d, Gut microbiotas conditioned on raw versus cooked tuber diets have differential impacts on host energy status. Gnotobiotic mice were colonized with gut microbiotas harvested from conventional donors fed raw versus cooked tuber (**a**, $n = 6$ animals per treatment, $n = 3$ germ-free controls per donor group; see Methods). Accounting for fivefold differences in caecal mass with colonization (**b**), a gut microbiota conditioned on a raw tuber diet had a significant impact on host energy status after 14 days, as indexed by change in body mass (**c**) and MRI-based body fat expressed relative to body mass (**d**). These effects suggest that the gut microbiota helped compensate for lower energetic returns on the raw tuber diet. Panels **b–d** reflect one data point per individual. Data are presented as mean ± s.e.m. and statistics reflect one-way ANOVA with Holm–Sidak correction for multiple comparisons. **e–i**, Consumption of raw versus cooked plant diets alters the gut microbiota in humans ($n = 8$, crossover design). Unweighted UniFrac principal coordinate plots (**e**) show that gut microbial communities clustered by individual. Study participants are represented by letters, coloured by diet phase, with the ellipse representing the participant-specific 95% confidence interval. Changes in gut microbial α-diversity (**f**) and β-diversity (**g**) versus baseline are indexed by Faith's phylogenetic distance and unweighted UniFrac distance, respectively. The plant-based diet affected both α-diversity and β-diversity, while cooking had significant effects on β-diversity alone. In **f** and **g**, individual participants are represented by letters, with the central ribbon representing the mean ± s.e.m., and statistics reflect linear mixed effect models analysing the effect of time on diet (P_{diet}) and its interaction with food preparation ($P_{cooking}$). Despite high correlations between operational taxonomic units (OTUs) that differed in abundance on raw and cooked diets (**h**), we detected 46 OTUs that differed uniquely on raw and 59 that differed uniquely on cooked. Colours reflect OTUs significantly affected by time on raw (orange), cooked (green) or both (blue) diets. Phylogenetic trees (**i**) summarizing 1,858 OTUs and internal nodes (phylogenetic isometric log transform) showed significant fold changes on the raw and cooked diet treatments. Clade taxonomy was assigned by a consensus naming scheme.

recipients (Supplementary Fig. 6c), highlighting the importance of host–microbial interactions for satiety[26,27].

To evaluate the relevance of these effects in humans, we fed healthy participants matched raw and cooked plant-based diets over two three-day diet interventions, in counterbalanced order (Supplementary Fig. 7a and Supplementary Table 1d,e). We observed no consistent differences in body mass, caloric or macronutrient intake between diets (Supplementary Fig. 7b–g and Supplementary Table 10). Gut microbial communities clustered strongly by participant (Fig. 4e), explaining >60% of variance, regardless of the distance metric used (Supplementary Table 11). Analyses of α-diversity and β-diversity that controlled for participant, the order of diet presentation and time on diet revealed a significant effect of the dietary intervention (Fig. 4f,g). Surprisingly, α-diversity decreased on our plant-based diets, potentially in response to the limited ingredients used and menu repetition across days. Treatment responses differed by participant, but across the cohort there was a significant effect of cooking on gut microbial β-diversity (Fig. 4g and Supplementary Fig. 8a–c). On cooked diets, changes in the gut microbiota were detectable within 48 h ($P=0.019$, linear mixed effect model with TukeyHSD) and persisted until day 5 ($P=0.019$) (Fig. 4g). However, the raw diet generated a later response, becoming significant at 72 h ($P=0.038$) and lingering for only 24 h post-intervention ($P=0.044$). Most diet-responsive OTUs were uniquely enriched on either raw or cooked diets, spanning multiple taxonomic groups (Fig. 4h,i).

Taken together, our results show that cooking plants rich in low-digestibility starch, a routine part of daily life, can have profound impacts on the gut microbiome, consistent with recent in vitro data[28]. Accordingly, future microbiome studies should control for or, at minimum, report food preparation alongside caloric and macronutrient content. The observation that everyday foods disrupt gut bacterial physiology when consumed raw raises opportunities for mining the human diet for therapeutics and prompts a polypharmacological view of the interactions between the gut microbiome and dietary small molecules[29]. Finally, these results emphasize that humans and our microbiomes were both affected by the adoption of habitual cooking, perhaps helping to explain accelerated gut microbial change in the human lineage[30] and encouraging steps toward a microbiome-informed understanding of human evolution.

Methods

Summary. Experiments were performed under the guidance of the Animal Care and Use Committee and the Committee on the Use of Human Subjects at Harvard University, and the Harvard Medical Area Standing Committee on Animals. To interrogate the impact of a cooked diet on the gut microbiome, we collected distal gut samples from conventional or gnotobiotic mice or human volunteers fed whole-food diets of plant items or meat served raw or cooked, or custom chows differing in starch digestibility or xenobiotic load. We used 16S rDNA sequencing with barcoded V4 primers (515F-806R) to assess gut microbial community structure, qPCR with these same primers or flow cytometry with fluorescent bead standards to assess community abundance, microbial RNAseq to assess gene transcription, gas chromatography to assess short-chain fatty acid production and fluorescent cell staining with PI and SYBR Green I to assess microbial physiology. 16S rDNA sequence data were processed using the Quantitative Insights into Microbial Ecology (QIIME) software package version 1.8.0[31], with microbial biomarker discovery performed using LEfSe[32] and/or linear mixed effects models[33] where appropriate. Microbial RNAseq data were analysed for differential expression using limma[34] with voom[35], with gene set enrichment analysis conducted via ROAST[36]. Fluorescence and scatter profiles were analysed in FlowJo following published protocols[19] to deliver proportions of bacterial cells with membrane damage (PI+) and distinct activity based on nucleic acid content, as measured with SYBR Green I. To probe food-derived compounds contributing to these effects, we profiled raw and cooked plant food extracts by mass spectrometry[37], using standards to confirm the identity of metabolites rendered differentially abundant by cooking.

Animal and human experiments. *Approvals.* Conventional mouse experiments were conducted in the Biological Research Infrastructure (BRI) barrier facility at Harvard University under the supervision of the Harvard University Animal Care and Use Committee (protocols #17-06-306 and #12-06). Gnotobiotic mouse experiments were conducted in the Gnotobiotics Core at Brigham & Women's Hospital under the supervision of the Harvard Medical Area Standing Committee on Animals (protocol #04805). Sample sizes for early animal experiments were determined based on prior findings of substantial diet-induced differences in hepatic gene expression[7]; sample sizes for follow-up studies were selected in reference to these initial experiments. Human experiments were conducted with informed written consent under the supervision of the Harvard University Committee on the Use of Human Subjects (protocol #IRB17-1016). Although blinding was not practical, core staff blind to the study hypotheses were responsible for the randomized assignment of conventional and gnotobiotic mice to cage, isolator and treatment groups. Our human experiments were performed based on a crossover design, with treatment order determined by computer-based randomization.

Gut microbial community structure and function in mice fed whole-food meat or tuber (WF) diets. We fed mice diets of meat or tuber served raw or cooked (1) to investigate the gut microbial impacts of consuming a whole-food diet in raw versus cooked form (Supplementary Fig. 1a) and (2) to validate that the murine gut microbial community responds rapidly and reproducibly to shifts in whole-food diets (Supplementary Notes). Male BALB/c mice ($n=24$, four sets of six littermates) were acquired from Charles River Laboratories at 21 days of age and co-housed with littermates under standard BRI conditions (ventilated cages including cob bedding and enrichment (no running wheels); ad libitum chow and water; 12 h light/dark cycle beginning at 6:00). At eight weeks of age, mice were housed individually in cages fitted with a wire mesh floor to minimize coprophagy. To prevent contamination and loss of diet beneath the mesh floor, diets were administered in Pyrex Petri dishes with weighted tops bearing four symmetrical feeding holes. Mice acclimated to this experimental set-up for three days before the start of diet manipulations. Diets consisted of organic lean beef eye round roast (*Bos taurus*) or organic orange-fleshed sweet potato tubers (*Ipomoea batatas* L. 'Beauregard') sourced fresh daily and served either raw, cooked or cooked but in a restricted ration that allowed us to evaluate the effects of a cooked diet given negative energy status. Full details of the food preparation procedure have been published elsewhere[7]. Briefly, for raw treatments, meat and tubers were sliced into standard cuboids and weighed into ad libitum rations (MRF, 20.0 ± 0.3 g; TRF, 40.0 ± 0.5 g). For cooked meat treatments, raw cuboids were weighed into rations (MCF, 20.0 ± 0.3 g; MCR, 10.0 ± 0.3 g) and roasted in covered Pyrex Petri dishes at 200 °C for 12 min, resulting in internal temperatures of 65–70 °C. For cooked tuber treatments, raw cuboids were weighed into rations (TCF, 40.0 ± 0.5 g, TCR, 20.0 ± 0.3 g) and roasted in foil packets at 204 °C for 25 min, a protocol confirmed by polarized light microscopy to gelatinize starch, then transferred into Pyrex Petri feeding dishes. Once cooled, diets were sealed with parafilm and fed within 3 h of preparation. Technical replicates prepared from the same starting materials were analysed for energy and macronutrient content using standard biochemical assays (Supplementary Table 1a). Mice were reared for five days on MRF, MCF, MCR, TRF, TCF or TCR diets ($n=4$ per diet), with littermates randomized symmetrically across diet groups. Diets were presented at the same time each day to give a standardized data collection cycle. During this daily intervention, mice were weighed during a period of inactivity and duplicate fresh faecal samples were collected and flash-frozen in liquid nitrogen. Food refusals from the past 24 h were collected, weighed to monitor fresh weight intake, and later freeze-dried to determine dry weight intake. At the end of the feeding trial, mice were fasted overnight (12 h) to promote consumption of food on demand. Two hours before euthanization, mice were presented with their assigned diets and in all cases began eating immediately. Body mass was taken immediately prior to euthanization via CO_2 inhalation. Duplicate ~200 mg samples of caecal effluent were collected within 3 min of death using sterile, RNase-free instruments and flash-frozen in liquid nitrogen. Faecal and caecal samples were stored at −80 °C until analysis. One mouse in the TRF group was euthanized after four days due to >20% weight loss, in accordance with our IACUC protocol; samples from this animal were excluded from all analyses.

Gut microbiota in mice fed chows differing in digestibility (DG) or xenobiotic (XB) load. We fed mice custom chows differing in starch digestibility (Supplementary Fig. 2a) or chlorogenic acid content (Supplementary Fig. 5f) to evaluate DG and XB load as potential mechanisms underlying the microbial changes observed on raw versus cooked tuber diets. C57BL/6J mice aged 6–12 weeks ($n=46$) were bred in-house and co-housed in groups of three to five under standard BRI conditions (see above) until their recruitment into a study. A total of 22 mice (12 male, 10 female) and 24 mice (12 male, 12 female) were used in the comparisons of starch digestibility or chlorogenic acid content, respectively. Before the study, mice were individually housed in standard ventilated cages with multiple forms of enrichment (nestlet, shack and cylinder; no running wheels) and allowed three days to acclimate to this set-up before the start of diet manipulations. We used custom semi-purified or grain-based chows manufactured by Envigo/Teklad (Supplementary Table 1b). DG chows were semi-purified and were matched in all ingredients except for the source of the starch fraction (50% wt/wt), which was known to be either highly resistant to mammalian amylases (LDS diet, based on high-amylose resistant starch; TD.140475) or highly susceptible (HDS diet, based on high-amylopectin waxy maize starch; TD.140474). XB chows represented

the inclusion or exclusion of 1% wt/wt chlorogenic acid (CGA; C3878, Sigma-Aldrich) in both grain-based low-fat and semi-purified high-fat diet conditions (LF, TD.96338; LF + CGA, TD.140472; HF, TD.08811; HF + CGA, TD.140473). All diets were irradiated by the manufacturer and stored in their original vacuum-sealed pouches until feeding. For sample collection, mice were reared for 28 days on LDS, HDS, LF, LF + CGA, HF or HF + CGA diets ($n = 6$–11 per diet), with littermates randomized symmetrically across groups in either the DG or XB trials. Just before the start of diet administration (day 0) and on days 1–3, 7, 14 and 28, mice were weighed during a period of inactivity, food weights were recorded to establish intake, and duplicate fresh faecal samples were collected and flash-frozen in liquid nitrogen. Faecal samples were stored at −80 °C until analysis. At the end of the feeding trial, mice were euthanized by cervical dislocation under isoflurane anaesthesia. We weighed the caecum both full and empty to assess the mass of caecal contents, and returned the empty caecum to the body cavity before storage at −80 °C. Analysis of body composition was performed on thawed carcasses at 37 °C via MRI scan (EchoMRI-700), after validating that this protocol closely replicated measurements obtained in vivo (Supplementary Notes).

Gut microbiota in mice fed six plant food (PF) diets. To confirm starch digestibility as a key mechanism shaping the gut microbial response to cooking, we fed mice raw or cooked versions of six common PFs varying in starch content and degree of starch digestibility (Supplementary Fig. 3a). Female six-week-old C57BL/6J mice ($n = 48$, four sets of 12 cagemates) were sourced from Jackson Laboratories. Mice were acclimated upon arrival to the BRI, during which they were cohoused under standard BRI conditions (see above). At the start of the experimental treatment, mice were individually housed in standard cages with bedding and enrichment (no running wheels) for the duration of the study. Diets were administered in plastic Petri dishes magnetically bound to the bottom of the cage. Cages were changed daily, and old cage bedding was saved to collect and weigh food refusals. Diets consisted of organic orange-fleshed sweet potato tubers (*Ipomoea batatas* L. 'Beauregard'), organic russet potato tubers (*Solanum tuberosum* 'Russet Burbank'), organic pre-frozen raw green peas (*Pisum sativum*), organic pre-frozen raw whole kernel sweetcorn (*Zea mays* convar. *Saccharata* var. *rugosa*), organic carrot (*Daucus carota* subsp. *sativus*) and organic beetroot (*Beta vulgaris*). Fresh vegetables were diced into standard cuboids (see above), and pre-frozen vegetables were thawed to room temperature. Diets were prepared fresh daily and served either raw or cooked. For raw treatments, all vegetables were weighed into unlimited rations (30.0 ± 0.9 g). For cooked treatments, all vegetables were weighed into ad libitum rations (30.0 ± 0.9 g) then roasted in individual foil packets for 25 min at 204 °C. Technical replicates were prepared for each dietary condition, sourced from the starting materials on each day of food preparation. For sample collection, mice were randomized symmetrically across diet treatments and reared for a minimum of three days on one of 12 diets: raw or cooked sweet potato, raw or cooked white potato, raw or cooked corn, raw or cooked peas, raw or cooked carrot, or raw or cooked beet ($n = 4$ animals per treatment). Diets were administered at the same time each day to allow for a standardized data collection schedule. During this time, mice were weighed, and duplicate fresh faecal samples were collected and flash-frozen in liquid nitrogen. Food refusals left in the Petri dish from the previous 24 h were collected and weighed, cages were changed, and old bedding was sifted for residual food refusals. Faecal samples were stored at −80 °C until analysis. We terminated the dietary intervention for the white potato, carrot and beet diet groups after three days due to >20% weight loss, in accordance with our IACUC protocol.

Microbial physiology. We used a validated flow cytometry assay[19] to evaluate the physiological consequences for the gut microbiota of raw versus cooked tuber diets (Fig. 3a) and two hypothetical candidates for the antimicrobial impact of raw tuber, chlorogenic acid and caffeic acid (Supplementary Fig. 5b). Female C57BL/6J mice aged 6–12 weeks (three sets of four littermates for the tuber experiment, three sets of three littermates for the antimicrobial candidate experiment) were bred in-house and co-housed in their litter groups under standard BRI conditions (see above). Before each study, mice were individually housed and allowed 24 h to acclimate to this set-up before the start of treatments. Within each study, littermates were randomized symmetrically across treatments. For sample collection, for the tuber experiment, mice were reared for four days on TRF, TCF, ad libitum chow or ad libitum chow plus 0.1% wt/wt pharmaceutical-grade ampicillin administered via water supply using light-shielded bottles. For the compound experiment, mice were reared for four days on ad libitum chow with a light-shielded water supply containing either 1% chlorogenic acid, 1% caffeic acid or no additive. Diets were presented at the same time each day to give a standardized data collection cycle, with compounds in water refreshed after two days. During this daily intervention, mice were weighed during a period of inactivity, and fresh faecal samples were collected into tubes flushed with CO_2 and transferred into an anaerobic chamber (Coy Laboratory Products) containing 5% H_2/10% CO_2/85% N_2 for immediate processing. All samples were processed within 10 min of production.

Gnotobiotic experiments. To establish the microbial consequences of diets under conditions in which the gut microbiota was tightly controlled, we conducted experiments with germ-free mice. Our experiments tested, respectively, the impacts on host net energy gain following inoculation with microbes pre-conditioned on raw versus cooked tuber diets (GB1; Fig. 4a) and the microbial response to LDS versus HDS diets in gnotobiotic mice conventionalized with a shared gut microbiota (GB2; Supplementary Fig. 2e). In each experiment, donor animals were eight-week-old conventionally raised C57BL/6J littermates that were bred and maintained under standard BRI conditions (GB1: females, $n = 2$; GB2: males, $n = 2$). Before their recruitment into the study, donors were individually housed and allowed three days to acclimate to this set-up before the start of diet manipulations (GB1) or euthanasia (GB2). In each experiment, recipient animals were male eight-week-old germ-free C57BL/6 mice that were bred and maintained under standard Gnotobiotics Core conditions (positive-pressure flexible film isolator with open-top cages containing cob bedding; no running wheels; ad libitum autoclaved chow and water; 12 h light/dark cycle beginning at 7:00) until their recruitment into studies at eight weeks of age (GB1: $n = 18$; GB2: $n = 24$). Mice sharing the same inoculation status were housed together in the same isolator and mice fed the same diet within an isolator were co-housed in groups of three. In GB1, donors were reared for four days on TRF ($n = 1$) or TCF ($n = 1$) diets, defined and prepared as described above. Each day, donors were weighed during a period of inactivity, food refusals from the past 24 h were collected and weighed to verify consumption, and duplicate fresh faecal samples were collected and flash-frozen in liquid nitrogen. In GB2, donors remained chow-fed until euthanasia. On the transplant day, donors were transported in their closed cages to the Gnotobiotics Core facility and euthanized via cervical dislocation under isoflurane anaesthesia. To minimize oxygen reaching the gut microbiota during preparation of the caecal-based inocula, haemostats were used to clamp just proximal and distal to caeca before their excision. Clamped caeca were immediately transferred into an anaerobic chamber (Coy Laboratory Products) containing 5% H_2/10% CO_2/85% N_2 and the inocula were prepared by diluting caecal contents 1:20 in reduced phosphate-buffered saline, vortexing to mix, spinning down and taking the supernatant. In GB1, within each group of germ-free mice receiving raw-conditioned or cooked-conditioned inocula, six recipients were gavaged with 200 µl of the live inoculum and three were gavaged with 200 µl of autoclaved inoculum (negative control) that was verified as inactive by culture. GB1 recipients were then maintained for 14 days on a standard gnotobiotic diet of autoclaved chow. In GB2, 12 germ-free recipients received 200 µl of live inoculum (pooled from two donor animals to ensure sufficient volume), six received 200 µl of autoclaved inoculum and six were not gavaged. Half of the recipients in each of these three colonization groups were maintained for 14 days on the LDS diet and the other half on the HDS diet. In both experiments, just before gavage (day 0) and on days 1–5, 8, 11 and 14, recipients were weighed, food intake was measured by subtraction from the previous hopper weight, and duplicate fresh faecal samples were collected and flash-frozen in liquid nitrogen. Faecal samples were stored at −80 °C until analysis. On day 14, mice were removed from their isolators and euthanized by cervical dislocation under isoflurane anaesthesia. The mass of caecal contents was assessed, and the carcass was retained (ex caecal effluent) for analysis of body composition by MRI.

Gut microbiota in humans fed raw and cooked plant-based diets (HC). To assess whether cooking alters the gut microbiota in humans, we fed volunteers matched plant-based meals served in raw and cooked forms, based on a counterbalanced crossover study design (Supplementary Fig. 7a). After obtaining written informed consent, we enrolled eight healthy adults (three men and five women) from within the Harvard University community. Participants were non-smokers with no history of gastrointestinal disease, allergy to diet ingredients or antibiotic use within 60 days of enrolment. Each participant completed two nine-day intervention arms, one involving raw foods and one involving cooked foods, with a one-month period between arms. The order of diet treatments was counterbalanced across participants and was determined by computer randomization at the time of study enrolment. We enlisted a professional chef to design a nutritionally adequate menu of plant-based (vegan, organic, gluten-free) meals and snacks that could be served in exclusively raw or exclusively cooked forms, with raw and cooked menus containing identical ingredients in identical proportions (Supplementary Fig. 7a and Supplementary Table 1d,e). We achieved dietary equivalence between raw and cooked menus (Supplementary Fig. 7d–g) by preparing mastermixes of all raw meal and snack components, reserving half of each mastermix for the raw treatment, and preparing the other half by roasting (lunch, dinner, nuts) or boiling (breakfast, smoothie, carrots) for the cooked treatment. All menu items were fed ad libitum, with food consumption determined by weighing refusals of all menu items separately. For each of two intervention arms, participants were asked to provide faecal samples on nine consecutive days: three prior to the start of the dietary intervention (wash-in period; days –2, 1, 0), when participants were consuming their habitual foods and beverages; three during the dietary intervention, when participants consumed only study-provided meals and snacks, plus water and up to one cup of black coffee or black tea per day; three following the dietary intervention (wash-out period: days 4, 5, 6), when participants returned to their habitual feeding and drinking patterns (Supplementary Fig. 8a). Participants kept detailed logs of food and beverage consumption for each nine-day intervention arm, and were weighed on each day of the dietary intervention, and these logs suggested strong compliance with the study protocol. Faecal samples were stored

for up to 24 h in a home freezer before being transferred to the lab for storage at −80 °C until analysis.

16S rDNA sequencing and analysis. Microbial DNA was isolated using the PowerSoil bacterial DNA extraction kit (MoBio) and PCR-amplified using barcoded universal bacterial primers targeting the V4 region of the 16S rRNA gene (515F and 806R). The following thermocycler protocol was used: 94 °C for 3 min, 35 cycles of 94 °C for 45 s, 50 °C for 30 s and 72 °C for 90 s, with a final extension at 72 °C for 10 min[38,39]. Triplicate reactions for each sample were pooled and amplification was confirmed by 1.5% gel electrophoresis. 16S rDNA amplicons were cleaned with AmpureXP beads (Agencourt), quantified using the Quant-iT Picogreen dsDNA Assay Kit (Invitrogen) and pooled evenly by DNA content. Pools were sequenced using the Illumina HiSeq (conventional mouse and human experiments) or MiSeq (gnotobiotic experiments) platforms, generating 2 × 100 bp (WF), 1 × 150 bp (DG, XB, PF, HC) or 250/150 bp (GB1, GB2) sequences (Supplementary Table 12). Sequences were analysed on the Harvard Odyssey and UCSF QB3 computational clusters using the QIIME (Quantitative Insights into Microbial Ecology) software package version 1.8.0[31]. OTUs were picked at 97% similarity against the Greengenes database[40], which we trimmed to span only the 16S rDNA region flanked by our sequencing primers (positions 521–773). We characterized a large number of reads per sample (WF, 174,582 ± 3,193; DG, 92,049 ± 1,864; XB, 86,774 ± 1,505; GB1, 29,733 ± 1,190; GB2, 33,159 ± 1,300; PF, 143,960 ± 4,082; HC, 42,772 ± 894). All sequences were used for the comparison of the relative abundance of bacterial taxonomic groups. To ensure unbiased generation of diversity metrics sensitive to sampling depth, each dataset was randomly subsampled at a depth that retained nearly all of the individual samples (WF, 50,000; DG, XB, 30,000; GB1, GB2, 15,000; PF, 40,924; HC, 19,339). Alpha diversity metrics were generated using either alpha_diversity.py (QIIME) or Vegan v2.5-2[41] and Picante v1.7[42] (R). Microbial biomarker discovery, as identified in text, was performed on the subsampled datasets using the LEfSe algorithm[32] after filtering out species-level OTUs with <100 sequences or present in only one sample and treating |linear discriminant analysis score| ≥ 2 as the threshold for significance. Permutation-based analyses of microbial community distances (ANOSIM, Adonis and PERMANOVA) were performed using compare_categories.py (QIIME) or the Adonis function of Vegan v2.5-2 (R), with 999 permutations per test. To avoid pseudoreplication in these tests, datasets were either trimmed to a single sample per subject, as specified in the text, or the participant/mouse identifiers were used as strata for permutation. In all cases, ANOSIM and PERMANOVA tests supported the same conclusions, so we report only ANOSIM results everywhere except the Supplementary Tables. For the PF experiment, longitudinal data were analysed using linear mixed effects models with the package lmerTest[33] and the formula y~Cooked*TimeOnDiet + (1|MouseID), where y represents the metric being tested. For the HC experiment, a similar formula was applied: y~Cooked*TimeOnDiet + Phase + (1|ParticipantID). In both experiments, the interaction between cooking and time on diet was taken to represent a significant difference between cooked and raw food consumption. Multiple testing correction was carried out with FDR correction (Benjamini–Hochberg). In both the PF and HC experiments: OTU-level abundance analysis was carried out using centred $\log_2$ transformation with count zero multiplicative replacement[43] before testing using linear mixed effects models. Phylogenetic node testing was carried out using the phylogenetic isometric log ratio transformation of PhILR version 1.6.0[44] after removal of OTUs not present in at least three samples with a total of 10 reads.

Microbial RNAseq. We conducted a metatranscriptomic analysis of microbial community-wide gene expression in caecal samples collected from mice fed whole-food diets of meat or tuber served raw or cooked. Caecal effluent was collected and flash-frozen in liquid nitrogen within 3 min of host death. Microbial cells were lysed by bead-beater (BioSpec Products), and total RNA was extracted with phenol:chloroform:isoamyl alcohol (pH 4.5, 125:24:1, Ambion 9720). Total RNA was purified using the Ambion MEGAClear Kit (Life Technologies) and rRNA was depleted via Ambion MICROBExpress subtractive hybridization (Life Technologies) and custom depletion oligonucleotides. The absence of genomic DNA contamination was confirmed by PCR with universal 16S primers (8F and 1391R). cDNA was synthesized using SuperScript II and random hexamers (Life Technologies), followed by second-strand synthesis with RNaseH and *Escherichia coli* DNA polymerase (New England Biolabs). Samples were fragmented enzymatically (E6040L and M0348S, New England Biolabs) and Illumina sequencing libraries were prepared on an Apollo 324 instrument using the PrepX mRNA Library Preparation Kit (WaferGen Biosystems). Libraries were quantified by qPCR on a Stratagene MX3000P qPCR System (Agilent) using ABsolute qPCR SYBR Green ROX Mix (Thermo Scientific). The size distribution of each library was quantified by an Agilent Bioanalyzer using an HS-DNA chip, and sample libraries were pooled evenly. The fully multiplexed pool was sequenced in three separate runs of an Illumina HiSeq (Supplementary Table 13), with strong reproducibility across runs (Supplementary Fig. 1d). To analyse the metatranscriptomic data, we quality controlled the FASTQ files with fastq-mcf[45] and removed rRNA reads using the database provided by SortMeRNA[46]. We removed host-originating reads by discarding sequences mapped by kallisto[47] to the mouse transcriptome (GRCm38.rel79). To obtain counts of KEGG[48] orthologues, we used translated search with DIAMOND[49] and retained results with an *E* value of <0.01. Our analyses were based on KEGG release 58.1. As a final cleaning step, matches to animal versions of KEGG orthology groups (KOs) were excluded, as were KOs associated with <1 read on average. Having obtained a set of KO counts for each sample, we then used the limma[34] package in R along with its voom[35] extension to evaluate differential expression while controlling for differences in sequencing depth and batch effects. The abundance metric used by limma is log counts per million, obtained by dividing the count of classified reads for each KEGG orthologue by the total number of reads submitted to DIAMOND for classification. Per-observation weights were generated by the voom procedure. To find higher-level patterns among the top genes, we ran gene set analyses with ROAST[36]. To visualize the dissimilarities between the metatranscriptomes, Ward. D2 hierarchical clustering was performed using a matrix of cosine distances and the hclust function in R. Before computing the distance matrix, batch effects resulting from sequencing replicates were removed with the limma package.

qPCR analysis. To quantify absolute bacterial abundance, we conducted qPCR using the same V4 primers employed in 16S rDNA sequencing (515F and 806R). For each reaction, template DNA at ~5 ng µl^{-1} was diluted 1:100, and 2 µl of this was combined with 12.5 µl ABsolute qPCR SYBR Green ROX Mix (Thermo Scientific), 6 µl nuclease-free H_2O and 2.25 µl of each primer (450 nM final concentration). The following program was run on a Stratagene MX3000P qPCR System (Agilent): 95 °C for 15 min, followed by 40 cycles of 95 °C for 15 s, 50 °C for 40 s and 72 °C for 30 s. A melting curve was performed after amplification to distinguish targeted and non-targeted PCR products. All reactions were performed in duplicate, with the mean value used for statistical analyses. Reaction concentrations were quantified against a standard curve created using serial twofold dilutions of pure culture *Akkermansia muciniphila* (DSM 22959) genomic DNA of known concentration plus a non-template control (all standard curves, $r^2 \geq 0.99$). Bacterial DNA per gram of faeces was determined by adjusting for the dilutions performed during DNA isolation (1:50), normalization to ~5 ng µl^{-1} (various) and qPCR set-up (1:100), and dividing this gross concentration by the grams of faeces utilized for the original DNA isolation (various). We report absolute bacterial community abundance in genome equivalents, where the murine gut microbiota was assigned a multiplier of 2.03×10^5 based on a mean genome size of 4.50 Mbp.

Short-chain fatty acid analysis. We used an established gas chromatography protocol[5] to measure the concentration of acetic, butyric and propionic acids in flash-frozen caecal samples collected from mice fed whole-food diets of meat or tuber. Briefly, samples of caecal effluent stored at −80 °C since harvest were thawed, weighed and resuspended in 400 µl of HPLC-grade water. Samples were homogenized and adjusted to pH 2–3 with 50% sulfuric acid. The acidified samples were incubated at room temperature for 5 min, with intermittent vortexing, then centrifuged for 10 min at 5,000*g*. A 300 µl volume of the clear supernatant was transferred into an Eppendorf tube, then 50 µl of the internal standard (1% 2-methylpentanoic acid solution) and 300 µl of anhydrous ethyl ether were added. The samples were vortexed for 30 s and centrifuged at 5,000*g* for 10 min. A 1 µl sample of the upper ether layer was used for analysis. Acids were identified and quantified in comparison to a reference mix of volatile acids, containing 10 mM concentrations of acetic, butyric and propionic acids (Matreya). The reference mix was validated against acid-specific standard curves to ensure quantification in the linear range. Results were expressed as mM concentrations per gram of sample, with the mean value across duplicate runs used for statistical analyses.

Bomb calorimetry analysis. Faecal pellets were collected from individual mice and lyophilized for 24 h before determination of energy content via bomb calorimetry. After completion of the drying process, 100–200 mg of dried stool was pressed into a pellet using a pellet press, and dried masses of the pressed pellets were recorded. Gross energy content was measured using an isoperibol oxygen bomb calorimeter with a semimicro oxygen bomb (models 6200 and 1109, respectively, Parr Instrument Co.). The calorimeter energy equivalent factor was determined using benzoic acid standards.

Microbial physiology analysis. Fresh faecal pellets were placed into an anaerobic chamber (Coy Laboratory Products) containing 5% H_2/10% CO_2/85% N_2 within 10 min of production. Bacterial physiology was assessed under anaerobic conditions according to validated protocols[19,20] using two fluorescent nucleic acid stains, propidium iodide (PI; Sigma-Aldrich) and SYBR Green I (Invitrogen) (Supplementary Notes). PI is excluded from bacterial cells with intact membranes due to its size and hydrophilicity, and therefore PI is commonly used to assess bacterial membrane damage[50]. SYBR Green I is used for total bacterial cell counts by flow cytometry, as it enters all bacteria irrespective of membrane status. Extensive data show that SYBR Green I-stained cells can be grouped into two clusters, low nucleic acid-containing (LNA) and high nucleic acid-containing (HNA) bacteria, according to their relative fluorescence and scatter characteristics[20,51]. Both groups have discernible biomass and activity levels, and within a given community HNA cells are considered to be more active than LNA cells[20,52,53]. Fresh faecal samples were stained for 10 min with PI at 0.04 mg ml^{-1}

final concentration (Sigma-Aldrich) or 15 min with SYBR Green I at 1× final concentration (Invitrogen). Fluorescent beads (3.4 µm, Spherotech) were added as an internal standard to determine cell abundance, and their density was determined for every flow cytometry analysis with Countbright beads (Invitrogen). All cytometric measurements were made using an LSRFortessa flow cytometer (Becton Dickinson) equipped with Coherent solid-state sapphire 100 mW 488 nm and 50 mW 561 nm lasers and a standard filter set-up. Data were analysed with FlowJo software version 7.6.3 (Tree Star).

In vitro bacterial growth assays. We selected for screening 15 gut bacterial isolates with high prevalence and abundance across 1,267 publicly available human faecal metagenomes[54], representing the five major phyla from the human gut (Bacteroidetes, Firmicutes, Actinobacteria, Proteobacteria and Verrucomicrobia). Strains were grown and assayed in brain–heart infusion (BHI) medium supplemented with L-cysteine hydrochloride (0.05% wt/vol), hemin (5 µg ml^{-1}), vitamin K (1 µg ml^{-1}) and resazurin (0.0001% wt/vol). Arginine-dependent *Eggerthella lenta* was grown and assayed in supplemented BHI plus arginine (1% wt/vol). Chlorogenic acid (Sigma-Aldrich) and caffeic acid (Sigma-Aldrich) were dissolved directly in BHI medium, while our positive control myricetin (TCI America) was dissolved in DMSO present at a final concentration of 1%. Minimum inhibitory concentration assays were performed using the broth microdilution method outlined by the Clinical Laboratory Standards Institute[55], with some changes. Briefly, assays were performed in triplicate in round-bottomed 96-well plates (Corning, Costar) in a final volume of 100 µl. Plates were prepared in an anaerobic chamber (Coy Laboratory Products) containing 5% H_2/10% CO_2/85% N_2 and were allowed to equilibrate for 3 h before bacteria were added. Inoculated plates were incubated at 37 °C for 24 h, with plates containing slow-growing *A. muciniphila* and *E. lenta* grown for 48 h. Absorbance values were measured at a wavelength of 600 nm ($A_{600\,nm}$) using a plate reader (Tecan). Relative growth was calculated by subtracting $A_{600\,nm}$ values from sterile controls and normalized to a growth control (BHI only or BHI plus 1% DMSO). Minimum inhibitory concentrations were defined as growth conditions that yielded a relative growth <0.1.

Metabolomics assays. Two different chromatography approaches were used to characterize the plant metabolites. Reverse phase chromatography was used for the non-polar metabolites, and this approach was complemented by normal phase chromatography with HILIC for polar metabolites and to characterize compounds either not retained or subject to matrix effects on the reverse phase column[56–60]. Raw and cooked samples of the six plant foods fed to mice in the PF study were reserved at the time of diet preparation and stored at −80 °C for metabolomics analysis. Raw and cooked foods were lyophilized to dryness and then powdered using a mortar and pestle. In a 2 ml screw-top tube, the powdered tissue was suspended in 80% MeOH/20% H_2O (0.2 g tissue per 1 ml of solvent). This suspension was vortexed for 30 s and then placed in an ultrasonicating bath at room temperature and sonicated for 30 min. The tube was vortexed for 30 s, after which it was centrifuged at 2,000 r.p.m. for 10 min. The supernatant was aspirated and stored at −20 °C until analysis. Extraction controls, containing only the extraction solvent, were also prepared. Before liquid chromatography–mass spectrometry (LC-MS) analysis, extracts were centrifuge-filtered (0.22 µm, UFC40GV0S, Millipore), transferred to glass vials, then methanol containing internal standards was added to each vial. For non-polar metabolite analysis, 2-amino-3-bromo-5-methylbenzoic acid was added to a final concentration of 1 µg ml^{-1}, and for polar metabolite analysis, ^{13}C-^{15}N labelled amino acids (767964, Sigma) were added to a final concentration of 15 µM. All chromatography was performed using an Agilent 1290 LC stack, with MS and tandem mass spectrometry (MS/MS) fragmentation data collected in both positive and negative ion mode using a Thermo QExactive (for HILIC) or Thermo QExactive HF (for C18) mass spectrometer (ThermoFisher Scientific). For each 2 µl sample injection, full MS spectra were acquired for *m/z* 80–1,200 at 60,000 resolution for C18, and *m/z* 70–1,050 at 70,000 resolution for HILIC, with fragmentation data acquired using stepped collision energies of 10, 20 and 40 eV at 17,500 resolution. Sample injection order was randomized and an injection blank of only methanol was run between samples. To detect non-polar metabolites, samples were chromatographically separated using a C18 column (Agilent ZORBAX Eclipse Plus C18, #959757, 50 mm × 2.1 mm, 1.8 µm) warmed to 60 °C with a flow rate of 0.4 ml min^{-1} equilibrated with 100% buffer A (100% LC-MS water w/ 0.1% formic acid) for 1 min, followed by a linear gradient to 100% buffer B (100% acetonitrile w/ 0.1% formic acid) at 8 min, and then isocratically held at 100% B for 1.5 min. To detect polar metabolites, samples were chromatographically separated using a HILIC column (Agilent InfinityLab Poroshell 120 HILIC-Z, #673775-924, 150 mm × 2.1 mm, 2.7 µm) warmed to 40 °C with a flow rate of 0.45 ml min^{-1} equilibrated with 100% buffer B (95:5 acetonitrile:water w/ 5 mM ammonium acetate) for 1 min, followed by a linear gradient diluting buffer B down to 89% with buffer A (100% water w/ 5 mM ammonium acetate and 5 µM methylene-di-phosphonic acid) over 10 min, then down to 70% B over 4.75 min, then down to 20% B over 0.5 min, and then isocratically held at 20% B for 2.25 min. The raw metabolomics data are available for download at https://opengut.ucsf.edu/CookingData.tar.gz.

Metabolomics analysis. Features—high-intensity signals narrowly contained at a given retention time and *m/z*—were detected using the MZMine software v 2.24[61]. Parameters for processing are contained in the original XML files used by MZMine (see Supplementary Data 1 and Supplementary Data 2 for negative and positive acquisition modes, respectively). Additional Python scripts were used to identify minimum and maximum retention time bounds for each peak, filter peaks that were not at least three times higher in a sample compared to all injection blanks, and filter peaks that did not have at least one MS/MS spectrum. Metabolite tables are provided in Supplementary Data 3 and Supplementary Data 4.

Metabolite identification. Chemical standards were used for identifications based on matching *m/z* better than 5 ppm, retention time difference <0.2 min for C18 and ≤0.5 for HILIC, and/or matching fragmentation patterns with a score of >0.5 as calculated by the Stein and Scott 'composite' algorithm[37] with modifications. Here, the mass weight term is set to 0, the intensity weight term is inversely proportional to the log of the number of aligned *m/z* values plus one, and the dot product and ratio of peak pair terms are averaged using the geometric mean. For each identification, peaks were integrated from a minimum to a maximum retention time and 5 ppm about a theoretical *m/z*. To complement the final identifications and processed data in Supplementary Table 7, we also provide the unfiltered initial compound identifications and raw peak heights (intensity) in Supplementary Data 5 (C18) and Supplementary Data 6 (HILIC). Compounds with a detected retention time of <1 min were excluded from subsequent analysis. For compounds detected by multiple chromatography methods or ionization modes we selected a single representative dataset based on intensity and prioritizing HILIC. When two or more chemical standards co-eluted, shared the same *m/z* value or were not distinguished by their fragmentation patterns, the ambiguity of the assigned identity was captured in the column 'unresolvable compounds' of Supplementary Table 7. For each identified compound, a measure of confidence is provided in Supplementary Table 7, comprising (1) the absolute value of the difference in retention time from the standard, (2) the mass error (ppm) of detected *m/z* versus theoretical *m/z* and (3) the MS/MS score comparing the experimental MS/MS fragmentation pattern to the standard. As defined by the Metabolomics Standards Initiative[62], any two of these orthogonal measures supports a level 1 identification for these non-novel metabolites. A total of 215 level 1 compounds were identified; 185 exceeded level 1 (high-confidence assignments by all three measures) and an additional 30 were categorized as 'unresolvable compounds' due to structural isomers. The identified compounds were added to Metabolite Atlas[63] to generate extracted ion chromatograms for each sample, shown together with matches between the experimental MS/MS spectra and the MS/MS spectrum of the chemical standard in Supplementary Data 7.

Differential metabolite analysis. A prior of 966.67 was added to all peak heights (two-thirds of the lowest non-zero abundance) before a $\log_2$ transformation. Then, FDR-corrected Welch's *t*-tests were carried out, with an FDR < 0.1 and an absolute $\log_2$ fold change of >1 considered to be significant. FDR was carried out within each analysis mode and plant food type. Ordination of metabolomics data was carried out using the ropls package[64]. The density heat maps were created using the stat_density_2d function of ggplot2[65] with 100 bins.

Statistical analysis. Statistical analyses and data visualization were performed in Prism 7 (GraphPad Software) and/or R version 3.5.0. Unless otherwise stated, to evaluate treatment effects where subjects were not explicitly matched across time points, we used unpaired *t*-tests, ANOVA or two-way ANOVA with Holm–Sidak correction for multiple comparisons. To compare across time points for the same individual, we used paired *t*-tests or repeated measures ANOVA with Holm–Sidak correction for multiple comparisons. All pairwise post-hoc comparisons were evaluated unless otherwise indicated. Non-parametric tests were employed when data violated the underlying assumption of normal distribution. Significance was set at $P < 0.05$ or FDR < 0.05 unless otherwise noted, with marginal results denoted by parentheses.

Reporting Summary. Further information on research design is available in the Nature Research Reporting Summary linked to this article.

Data availability

16S rDNA and RNA sequencing data have been deposited in the NCBI Sequence Read Archive under accession no. PRJNA504908. Metabolomics raw data are available for download at https://opengut.ucsf.edu/CookingData.tar.gz. Figure source data and additional study data are available on request from the corresponding authors.

Received: 17 March 2019; Accepted: 23 August 2019;
Published online: 30 September 2019

References

1. Carmody, R. N. et al. Diet dominates host genotype in shaping the murine gut microbiota. *Cell Host Microbe* **17**, 72–84 (2015).

2. Muegge, B. D. et al. Diet drives convergence in gut microbiome functions across mammalian phylogeny and within humans. *Science* **332**, 970–974 (2011).
3. Smits, S. A. et al. Seasonal cycling in the gut microbiome of the Hadza hunter-gatherers of Tanzania. *Science* **357**, 802–806 (2017).
4. Turnbaugh, P. J. et al. The effect of diet on the human gut microbiome: a metagenomic analysis in humanized gnotobiotic mice. *Sci. Transl. Med.* **1**, 6ra14 (2009).
5. David, L. A. et al. Diet rapidly and reproducibly alters the human gut microbiome. *Nature* **505**, 559–563 (2014).
6. Carmody, R. N. & Wrangham, R. W. The energetic significance of cooking. *J. Hum. Evol.* **57**, 379–391 (2009).
7. Carmody, R. N. et al. Genetic evidence of human adaptation to a cooked diet. *Genome Biol. Evol.* **8**, 1091–1103 (2016).
8. Snow, P. & O'Dea, K. Factors affecting the rate of hydrolysis of starch in food. *Am. J. Clin. Nutr.* **34**, 2721–2727 (1981).
9. Ze, X., Duncan, S. H., Louis, P. & Flint, H. J. *Ruminococcus bromii* is a keystone species for the degradation of resistant starch in the human colon. *ISME J.* **6**, 1535 (2012).
10. Cowan, M. M. Plant products as antimicrobial agents. *Clin. Microbiol. Rev.* **12**, 564–582 (1999).
11. Witte, W. Medical consequences of antibiotic use in agriculture. *Science* **279**, 996–997 (1998).
12. Carmody, R. N., Weintraub, G. S. & Wrangham, R. W. Energetic consequences of thermal and nonthermal food processing. *Proc. Natl Acad. Sci. USA* **108**, 19199–19203 (2011).
13. Guan, Y., Wu, T., Lin, M. & Ye, J. Determination of pharmacologically active ingredients in sweet potato (*Ipomoea batatas* L.) by capillary electrophoresis with electrochemical detection. *J. Agric. Food Chem.* **54**, 24–28 (2006).
14. Salyers, A. A., Vercellotti, J. R., West, S. E. & Wilkins, T. D. Fermentation of mucin and plant polysaccharides by strains of *Bacteroides* from the human colon. *Appl. Environ. Microbiol.* **33**, 319–322 (1977).
15. Martens, E. C. et al. Recognition and degradation of plant cell wall polysaccharides by two human gut symbionts. *PLoS Biol.* **9**, e1001221 (2011).
16. Sun, T., Laerke, H. N., Jorgenson, H. & Knudsen, K. E. B. The effect of extrusion cooking of different starch sources on the in vitro and in vivo digestibility in growing pigs. *Anim. Feed Sci. Technol.* **131**, 66–85 (2006).
17. Warren, F. J. et al. Food starch structure impacts gut microbiome composition. *mSphere* **3**, e00086–00018 (2018).
18. Livesey, G. The impact of complex carbohydrates on energy balance. *Eur. J. Clin. Nutr.* **49**, 89S–96S (1995).
19. Maurice, C. F., Haiser, H. J. & Turnbaugh, P. J. Xenobiotics shape the physiology and gene expression of the active human gut microbiome. *Cell* **152**, 39–50 (2013).
20. Maurice, C. F. & Turnbaugh, P. J. Quantifying and identifying the active and damaged subsets of indigenous microbial communities. *Methods Enzym.* **531**, 91–107 (2013).
21. Borges, A., Ferreira, C., Saavedra, M. J. & Simoes, M. Antibacterial activity and mode of action of ferulic and gallic acids against pathogenic bacteria. *Microb. Drug Resist.* **19**, 256–265 (2013).
22. Lou, Z. et al. p-Coumaric acid kills bacteria through dual damage mechanisms. *Food Control* **25**, 550–554 (2012).
23. Alves, M. J. et al. Antimicrobial activity of phenolic compounds identified in wild mushrooms, SAR analysis and docking studies. *J. Appl. Microbiol.* **115**, 346–357 (2013).
24. Cho, I. et al. Antibiotics in early life alter the murine colonic microbiome and adiposity. *Nature* **488**, 621–626 (2012).
25. Butaye, P., Devriese, L. A. & Haesebrouck, F. Antimicrobial growth promoters used in animal feed: effects of less well known antibiotics on Gram-positive bacteria. *Clin. Microbiol. Rev.* **16**, 175–188 (2003).
26. Vijay-Kumar, M. et al. Metabolic syndrome and altered gut microbiota in mice lacking toll-like receptor 5. *Science* **328**, 228–231 (2010).
27. Breton, J. et al. Gut commensal *E. coli* proteins activate host satiety pathways following nutrient-induced bacterial growth. *Cell Metab.* **23**, 324–334 (2016).
28. Perez-Burillo, S. et al. Effect of food thermal processing on the composition of the gut microbiota. *J. Agric. Food Chem.* **66**, 11500–11509 (2018).
29. Koppel, N., Maini Rekdal, V. & Balskus, E. P. Chemical transformation of xenobiotics by the human gut microbiota. *Science* **356**, eaag2770 (2017).
30. Moeller, A. H. et al. Rapid changes in the gut microbiome during human evolution. *Proc. Natl Acad. Sci. USA* **111**, 16431–16435 (2014).
31. Caporaso, J. G. et al. QIIME allows analysis of high-throughput community sequencing data. *Nat. Methods* **7**, 335–336 (2010).
32. Segata, N. et al. Metagenomic biomarker discovery and explanation. *Genome Biol.* **12**, 1–18 (2011).
33. Kuznetsova, A., Brockhoff, P. B. & Christensen, R. H. B. lmerTest package: tests in linear mixed effects models. *J. Stat. Softw.* **82**, 1–26 (2017).
34. Ritchie, M. E. et al. limma powers differential expression analyses for RNA-sequencing and microarray studies. *Nucleic Acids Res.* **43**, e47 (2015).
35. Law, C. W., Chen, Y., Shi, W. & Smyth, G. K. voom: precision weights unlock linear model analysis tools for RNA-seq read counts. *Genome Biol.* **15**, 1–17 (2014).
36. Wu, D. et al. ROAST: rotation gene set tests for complex microarray experiments. *Bioinformatics* **26**, 2176–2182 (2010).
37. Stein, S. E. & Scott, D. R. Optimization and testing of mass spectral library search algorithms for compound identification. *J. Am. Soc. Mass Spectrom.* **5**, 859–866 (1994).
38. Caporaso, J. G. et al. Ultra-high-throughput microbial community analysis on the Illumina HiSeq and MiSeq platforms. *ISME J.* **6**, 1621–1624 (2012).
39. Caporaso, J. G. et al. Global patterns of 16S rRNA diversity at a depth of millions of sequences per sample. *Proc. Natl Acad. Sci. USA* **108**, 4516–4522 (2011).
40. DeSantis, T. Z. et al. Greengenes, a chimera-checked 16S rRNA gene database and workbench compatible with ARB. *Appl. Environ. Microbiol.* **72**, 5069–5072 (2006).
41. vegan: Community Ecology Package, R package v. 2.5-2 (cran.R-project, 2018); https://CRAN.R-project.org/package=vegan
42. Kembel, S. W. et al. Picante: R tools for integrating phylogenies and ecology. *Bioinformatics* **26**, 1463–1464 (2010).
43. Gloor, G. B., Macklaim, J. M., Pawlowsky-Glahn, V. & Egozcue, J. J. Microbiome datasets are compositional: and this is not optional. *Front. Microbiol.* **8**, 2224 (2017).
44. Silverman, J. D., Washburne, A. D., Mukherjee, S. & David, L. A. A phylogenetic transform enhances analysis of compositional microbiota data. *eLife* **6**, e21887 (2017).
45. Aronesty, E. Comparison of sequencing utility programs. *Open Bioinforma. J.* **7**, 1–8 (2013).
46. Kopylova, E., Noé, L. & Touzet, H. SortMeRNA: fast and accurate filtering of ribosomal RNAs in metatranscriptomic data. *Bioinformatics* **28**, 3211–3217 (2012).
47. Bray, N. L., Pimentel, H., Melsted, P. & Pachter, L. Near-optimal probabilistic RNA-seq quantification. *Nat. Biotechnol.* **34**, 525–527 (2016).
48. Kanehisa, M. et al. KEGG for linking genomes to life and the environment. *Nucleic Acids Res.* **36**, D480–D484 (2008).
49. Buchfink, B., Xie, C. & Huson, D. H. Fast and sensitive protein alignment using DIAMOND. *Nat. Methods* **12**, 59–60 (2015).
50. Strauber, H. & Muller, S. Viability states of bacteria: specific mechanisms of selected probes. *Cytometry A* **77**, 623–634 (2010).
51. Bouvier, T., Del Giorgio, P. A. & Gasol, J. M. A comparative study of the cytometric characteristics of high and low nucleic-acid bacterioplankton cells from different aquatic ecosystems. *Environ. Microbiol.* **9**, 2050–2066 (2007).
52. Gasol, J. M., Zweifel, U. L., Peters, F., Fuhrman, J. A. & Hagström, Å. Significance of size and nucleic acid content heterogeneity as measured by flow cytometry in natural planktonic bacteria. *Appl. Environ. Microbiol.* **65**, 4475–4483 (1999).
53. Lebaron, P., Servais, P., Agogue, H., Courties, C. & Joux, F. Does the high nucleic acid content of individual bacterial cells allow us to discriminate between active cells and inactive cells in aquatic systems? *Appl. Environ. Microbiol.* **67**, 1775–1782 (2001).
54. Nayfach, S., Fischbach, M. A. & Pollard, K. S. MetaQuery: a web server for rapid annotation and quantitative analysis of specific genes in the human gut microbiome. *Bioinformatics* **31**, 3368–3370 (2015).
55. CLSI. *Methods for Dilution Antimicrobial Susceptibility Tests for Bacteria That Grow Aerobically; Approved Standard* 9th edn (Clinical and Laboratory Standards Institute, 2012).
56. Want, E. J. et al. Global metabolic profiling procedures for urine using UPLC-MS. *Nat. Protoc.* **5**, 1005–1018 (2010).
57. Dunn, W. B. et al. Procedures for large-scale metabolic profiling of serum and plasma using gas chromatography and liquid chromatography coupled to mass spectrometry. *Nat. Protoc.* **6**, 1060–1083 (2011).
58. Ivanisevic, J. et al. Toward 'omic scale metabolite profiling: a dual separation-mass spectrometry approach for coverage of lipid and central carbon metabolism. *Anal. Chem.* **85**, 6876–6884 (2013).
59. Mahieu, N. G., Spalding, J. L., Gelman, S. J. & Patti, G. J. Defining and detecting complex peak relationships in mass spectral data: the mz.unity algorithm. *Anal. Chem.* **88**, 9037–9046 (2016).
60. Bowen, B. P. & Northen, T. R. Dealing with the unknown: metabolomics and metabolite atlases. *J. Am. Soc. Mass Spectrom.* **21**, 1471–1476 (2010).
61. Katajamaa, M., Miettinen, J. & Orešič, M. MZmine: toolbox for processing and visualization of mass spectrometry based molecular profile data. *Bioinformatics* **22**, 634–636 (2006).
62. Sumner, L. W. et al. Proposed minimum reporting standards for chemical analysis. *Metabolomics* **3**, 211–221 (2007).
63. Yao, Y. et al. Analysis of metabolomics datasets with high-performance computing and metabolite atlases. *Metabolites* **5**, 431–442 (2015).
64. Thevenot, E. A., Roux, A., Xu, Y., Ezan, E. & Junot, C. Analysis of the human adult urinary metabolome variations with age, body mass index and gender

by implementing a comprehensive workflow for univariate and OPLS statistical analyses. *J. Proteome Res.* **14**, 3322–3335 (2015).
65. Wickham, H. *ggplot2: Elegant Graphics for Data Analysis* (Springer, 2016).

Acknowledgements

We are indebted to R. Dutton and R. Wrangham for pivotal discussions, to T. Herfel, B. Mickelson, N. Pai and C. Pelkman for help with diet development, to L. Bry, A. Bustion, M. Correa, C. Daly, M. Delaney, L. Deng, O. Erbilgin, A. Freedman, E. Groopman, S. Kosina, F. Pontiggia, C. Reardon, J. Thomas and V. Yeliseyev for technical assistance and to E. Balskus, L. David, R. Losick and R. Nayak for comments on the manuscript. This work was supported by the National Institutes of Health (P.J.T., R01HL122593; R.N.C., F32DK101154), Boston Nutrition Obesity Research Center, Leakey Foundation, G.W. Hooper Foundation, Harvard Dean's Competitive Fund for Promising Scholarship, William F. Milton Fund, the Defense Advanced Research Projects Agency (T.R.N., HR0011516183) and the UCSF Department of Microbiology and Immunology. J.E.B. was the recipient of a Natural Sciences and Engineering Research Council of Canada Postdoctoral Fellowship. P.J.T. is a Chan Zuckerberg Biohub investigator and a Nadia's Gift Foundation Innovator supported, in part, by the Damon Runyon Cancer Research Foundation (DRR-42-16) and the Searle Scholars Program (SSP-2016-1352).

Author contributions

R.N.C. and P.J.T. designed the study. R.N.C. and K.S.C. performed the animal experiments. R.N.C., K.S.C. and V.M.R. performed the human experiments. R.N.C., J.E.B., K.S.C. and P.J.T. performed 16S rDNA sequencing and/or associated data analysis. R.N.C. and J.E.B. performed qPCR and associated data analysis. R.N.C., J.E.B., S.L., K.S.P. and P.J.T. performed microbial RNA sequencing and/or associated data analysis. Q.Y.A. performed bomb calorimetry. J.E.B., B.P.B., K.B.L., D.T., E.N.B., T.R.N. and P.J.T. performed metabolomics assays and/or associated data analysis. C.F.M. and K.C.B. performed microbial physiology assays and associated data analysis. P.S. performed in vitro growth experiments and associated data analysis. T.W.B. validated and performed measurements of body composition in mice. R.N.C., J.E.B. and P.J.T. wrote the manuscript with input from all co-authors.

Competing interests

The authors declare no competing interests.

Additional information

Supplementary information is available for this paper at https://doi.org/10.1038/s41564-019-0569-4.

Correspondence and requests for materials should be addressed to R.N.C. or P.J.T.

Reprints and permissions information is available at www.nature.com/reprints.

Publisher's note Springer Nature remains neutral with regard to jurisdictional claims in published maps and institutional affiliations.

nature research

Corresponding author(s): Peter J. Turnbaugh and Rachel N. Carmody

Last updated by author(s): Jul 24, 2019

Reporting Summary

Nature Research wishes to improve the reproducibility of the work that we publish. This form provides structure for consistency and transparency in reporting. For further information on Nature Research policies, see Authors & Referees and the Editorial Policy Checklist.

Statistics

For all statistical analyses, confirm that the following items are present in the figure legend, table legend, main text, or Methods section.

n/a	Confirmed
☐	☒ The exact sample size (*n*) for each experimental group/condition, given as a discrete number and unit of measurement
☐	☒ A statement on whether measurements were taken from distinct samples or whether the same sample was measured repeatedly
☐	☒ The statistical test(s) used AND whether they are one- or two-sided *Only common tests should be described solely by name; describe more complex techniques in the Methods section.*
☐	☒ A description of all covariates tested
☐	☒ A description of any assumptions or corrections, such as tests of normality and adjustment for multiple comparisons
☐	☒ A full description of the statistical parameters including central tendency (e.g. means) or other basic estimates (e.g. regression coefficient) AND variation (e.g. standard deviation) or associated estimates of uncertainty (e.g. confidence intervals)
☐	☒ For null hypothesis testing, the test statistic (e.g. *F*, *t*, *r*) with confidence intervals, effect sizes, degrees of freedom and *P* value noted *Give P values as exact values whenever suitable.*
☒	☐ For Bayesian analysis, information on the choice of priors and Markov chain Monte Carlo settings
☐	☒ For hierarchical and complex designs, identification of the appropriate level for tests and full reporting of outcomes
☐	☒ Estimates of effect sizes (e.g. Cohen's *d*, Pearson's *r*), indicating how they were calculated

Our web collection on statistics for biologists contains articles on many of the points above.

Software and code

Policy information about availability of computer code

Data collection	No software was used to collect data in this study.
Data analysis	16S rDNA sequencing data were analyzed using QIIME (version 1.8.0), LEfSe (version 1.0), and various R packages, as indicated in the text. Microbial RNA sequencing data were analyzed using packages available from GitHub (fastq-mcf, SortMeRNA, kallisto, DIAMOND) and R Bioconductor, as indicated in the text. Physiological cell staining data were analyzed using FlowJo software (version 7.6.3). Metabolomics data were analyzed in MZMine (version 2.24) according to parameters uploaded as Supplementary Data 1 and 2 for negative and positive acquisition mode, respectively. All other analyses were performed in GraphPad Prism (version 7.0e) or R (version 3.5.0).

For manuscripts utilizing custom algorithms or software that are central to the research but not yet described in published literature, software must be made available to editors/reviewers. We strongly encourage code deposition in a community repository (e.g. GitHub). See the Nature Research guidelines for submitting code & software for further information.

Data

Policy information about availability of data

All manuscripts must include a data availability statement. This statement should provide the following information, where applicable:

- Accession codes, unique identifiers, or web links for publicly available datasets
- A list of figures that have associated raw data
- A description of any restrictions on data availability

16S rDNA and RNA sequencing data were deposited in the NCBI Sequence Read Archive under accession PRJNA504908. Metabolomics raw data are available for download at https://opengut.ucsf.edu/CookingData.tar.gz. Figure source data and additional study data are available by request (carmody@fas.harvard.edu or peter.turnbaugh@ucsf.edu).

Field-specific reporting

Please select the one below that is the best fit for your research. If you are not sure, read the appropriate sections before making your selection.

☒ Life sciences ☐ Behavioural & social sciences ☐ Ecological, evolutionary & environmental sciences

For a reference copy of the document with all sections, see nature.com/documents/nr-reporting-summary-flat.pdf

Life sciences study design

All studies must disclose on these points even when the disclosure is negative.

Sample size	No statistical methods were employed to predetermine sample sizes. Sample sizes for the initial WF study were based on prior findings of substantial diet-induced differences in hepatic gene expression in these same animals (ref. 7); sample sizes for follow-up studies targeting underlying mechanisms were selected in reference to the WF study.
Data exclusions	The following exclusions are noted in the Methods: In the WF study, one mouse in the TRF treatment group was euthanized after 4 days due to >20% weight loss, in accordance with our IACUC protocol; samples from this animal were excluded from all analyses. In the PF study, we terminated the dietary intervention for the white potato, carrot, and beet diet groups after 3 of 4 planned days due to >20% weight loss, in accordance with our IACUC protocol.
Replication	We have taken several steps to evaluate the reproducibility of our experiments. First, for the focal dietary contrast involving raw versus cooked tuber, we performed four independent feeding trials that resulted in consistent effects (WF, PF, GB1 donors, microbial physiology). Second, we performed two independent experiments testing the impact of starch digestibility on the gut microbiota, one in conventional mice (DG) and one in gnotobiotic mice colonized from a common donor (GB2), with both experiments showing the same effects. Third, we performed feeding trials across a range of starch-rich and low-starch foods (PF), which further confirmed starch digestibility as a key driver shaping the gut microbial impacts of cooking. Fourth, we performed HILIC as well as C18 chromatography, using both metabolomics datasets to refine our compounds of interest. Finally, we demonstrated that the impact of cooking was detectable in both mice and humans fed raw versus cooked plant diets, and, to establish broader parallels in dietary responsiveness, we verified parallel gut microbial responses in mice and humans fed plant-based versus animal-based diets, as described in the Supplementary Notes.
Randomization	To control for variation in baseline gut microbial communities, all conventional mouse studies employed distribution of former cagemates across treatment groups, with the assignment to treatment groups determined randomly by computer. Random allocation of gnotobiotic mice to treatment groups was performed by Core facility staff blinded to the study hypotheses. Human studies evaluating raw versus cooked plant based diets employed a counterbalanced crossover study design, where the order of treatments was determined randomly by computer.
Blinding	Our conventional mouse, gnotobiotic mouse, and human diet experiments did not involve blinding, except in the assignment of animals to treatment groups, as noted above. Blinding was not practical in these studies in part because small teams of 1-3 researchers performed all end-to-end duties associated with these experiments (including study planning, recruitment, diet preparation, sample and data collection), and in part because there were visible and olfactory differences among food substrates and their raw versus cooked preparations.

Reporting for specific materials, systems and methods

We require information from authors about some types of materials, experimental systems and methods used in many studies. Here, indicate whether each material, system or method listed is relevant to your study. If you are not sure if a list item applies to your research, read the appropriate section before selecting a response.

Materials & experimental systems

n/a	Involved in the study
☒	☐ Antibodies
☒	☐ Eukaryotic cell lines
☒	☐ Palaeontology
☐	☒ Animals and other organisms
☐	☒ Human research participants
☒	☐ Clinical data

Methods

n/a	Involved in the study
☒	☐ ChIP-seq
☐	☒ Flow cytometry
☒	☐ MRI-based neuroimaging

Animals and other organisms

Policy information about studies involving animals; ARRIVE guidelines recommended for reporting animal research

Laboratory animals	Our study involved multiple experiments on conventional and gnotobiotic mice. Details on the animals used are listed below, organized by study. WF: Conventional BALB/c mice, males, 8 weeks of age, n=24 (4 sets of 6 littermates) DG: Conventional C57BL/6J mice, males and females, 6-12 weeks of age, n=22 (12 male, 10 female) XB: Conventional C57BL/6J mice, males and females, 6-12 weeks of age, n=24 (12 male, 12 female)

	PF: Conventional C57BL/6J mice, females, 6 weeks of age, n=48 (4 sets of 12 cagemates) Microbial physiology, tuber: Conventional C57BL/6J mice, females, 6-12 weeks of age, n=12 (3 sets of 4 littermates) Microbial physiology, xenobiotics: Conventional C57BL/6J mice, females, 6-12 weeks of age, n=9 (3 sets of 3 littermates) GB1, donors: Conventional C57BL/6J mice, females, 8 weeks of age, n=2 (littermates) GB1, recipients: Germ-free C57BL/6 mice, males, 8 weeks of age, n=18 (housed in 3 isolators) GB2, donors: Conventional C57BL/6J mice, males, 8 weeks of age, n=2 (littermates) GB2, recipients: Germ-free C57BL/6 mice, males, 8 weeks of age, n=24 (housed in 3 isolators)
Wild animals	Our study did not involve wild animals.
Field-collected samples	Our study did not involve samples collected from the field.
Ethics oversight	Conventional mouse experiments were conducted in the Biological Research Infrastructure (BRI) barrier facility at Harvard University under the approval and supervision of the Harvard University Animal Care and Use Committee (Protocol #17-06-306 and #12-06). Gnotobiotic mouse experiments were conducted in the Gnotobiotics Core at Brigham & Women's Hospital under the approval and supervision of the Harvard Medical Area Standing Committee on Animals (Protocol #04805).

Note that full information on the approval of the study protocol must also be provided in the manuscript.

Human research participants

Policy information about studies involving human research participants

Population characteristics	Our human study participants were healthy women (n=5) and men (n=3) in the Harvard University community, ranging in age from 24-40. Participants were non-smokers with no history of gastrointestinal disease, allergy to diet ingredients, or antibiotic use within 60 days of enrollment or during the study. Our human study was conducted based on a counterbalanced crossover study design, with treatment order randomized across participants. All data characterizing gut microbial community responses to raw versus cooked plant diets were analyzed within-subjects, using individual participants as their own controls.
Recruitment	Participants were recruited by email and poster from within the Harvard University community. Students, advisees, and employees of the study PI (Carmody) were excluded from participation, in accordance with our IRB protocol. Self-selection and other potential recruitment biases are unlikely to impact our results because our human research employed a within-subjects design, meaning that each participant served as their own control in all analyses of dietary impacts on gut microbial response.
Ethics oversight	Human experiments were conducted with informed written consent under the approval and supervision of the Harvard University Committee on the Use of Human Subjects (Protocol #IRB17-1016).

Note that full information on the approval of the study protocol must also be provided in the manuscript.

Flow Cytometry

Plots

Confirm that:

☒ The axis labels state the marker and fluorochrome used (e.g. CD4-FITC).

☒ The axis scales are clearly visible. Include numbers along axes only for bottom left plot of group (a 'group' is an analysis of identical markers).

☒ All plots are contour plots with outliers or pseudocolor plots.

☒ A numerical value for number of cells or percentage (with statistics) is provided.

Methodology

Sample preparation	Fresh fecal samples were handled in an anaerobic chamber throughout sample preparation. Samples were diluted 1:10 (w:v) in reduced PBS. Samples were centrifuged at 700 RCF for 1 min to separate large organic debris, the bacterial supernatant was washed 3 times by repeated centrifugations of 3 min at 6,000 RCF and resuspension in rPBS, before further dilution and individual staining with PI or SYBRGreenI. Diluted samples were individually stained for 10 min with PI at 0.04 mg/mL final concentration (Sigma-Aldrich) or 15 min with SYBRGreenI at 1X final concentration (Invitrogen). Fluorescent beads (3.4 µm, Spherotech) were added as an internal standard to determine cell abundance, and their density was determined for every flow cytometry analysis with Countbright beads (Invitrogen). All samples were stained and run in triplicate.
Instrument	LSRFortessa flow cytometer (Becton Dickinson) equipped with solid-state Coherent Sapphire 100 mW 488 nm and 50 mW 561 nm lasers, and standard filter setup. Acquisition plots were log-scaled and the number of events was below 1,200 events/s.
Software	FlowJo software version 7.6.3 (Tree Star)
Cell population abundance	We converted the number of gated events into cell abundances using the following equation: (Vb x Cb x Ec) / (Eb x Vs) where Vb = bead volume, Cb = bead concentration, Ec = cell events, Eb = bead events, and Vs= total volume of the sample. Using the total SYBRGreenI positive cells as the total bacterial abundance, we then calculated the relative proportion of cells in each physiological category [i.e. PI+ cells, HNA cells, and low nucleic acid (LNA) cells].
Gating strategy	Gates were identified using a combination of dot plots, contour plots, zebra plots, and pseudocolor plots to ensure adequate identification of populations of interest. We gated the cells of interest according to their Side Scatter (SSC) and respective

fluorescence emission channels: PI+ cells were gated based on their higher red fluorescence relative to non-PI cells (PE-Texas Red channel), and HNA and LNA cells were gated relative to each other based on their respective levels of green fluorescence (FITC channel). Once the bead and cell gates were made, they were batch-applied to all samples to limit variability, and we confirmed the gates for each sample manually. We also gated the reference beads that were present in every sample acquired, excluding bead doublets and triplets. We controlled for variation in the flow cytometry signals using the fluorescence and scatter values of the reference beads.

☒ Tick this box to confirm that a figure exemplifying the gating strategy is provided in the Supplementary Information.